Science Signaling

Special Issue

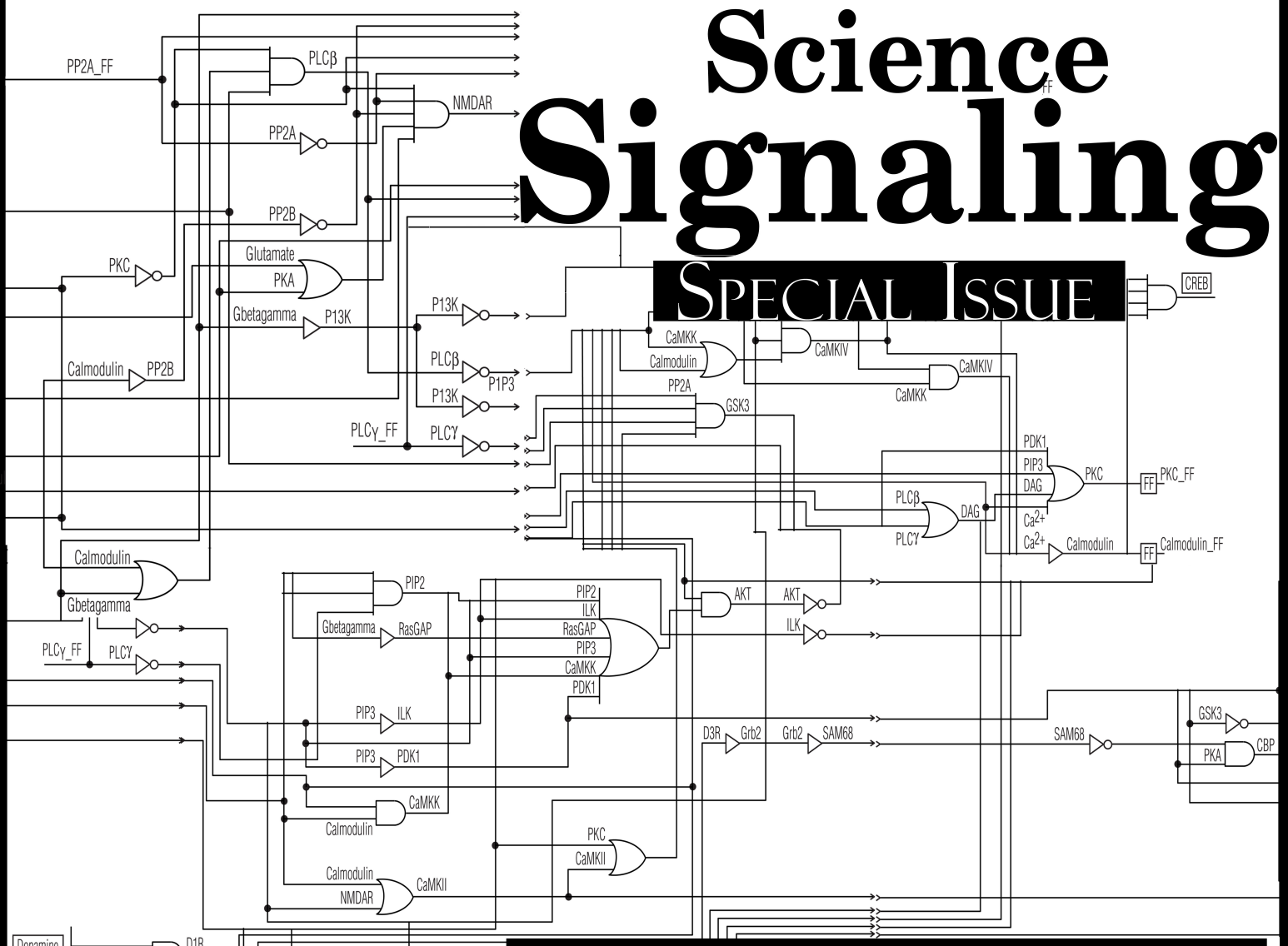

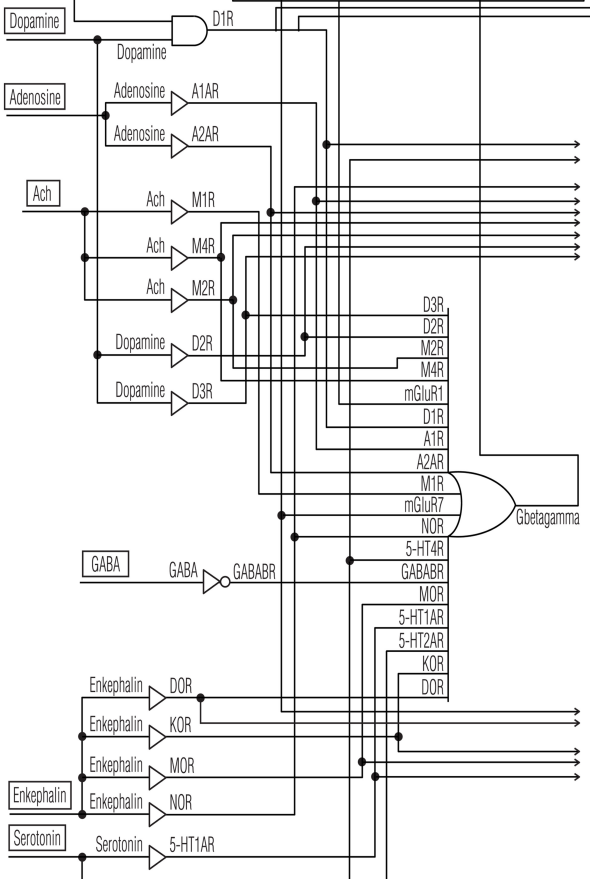

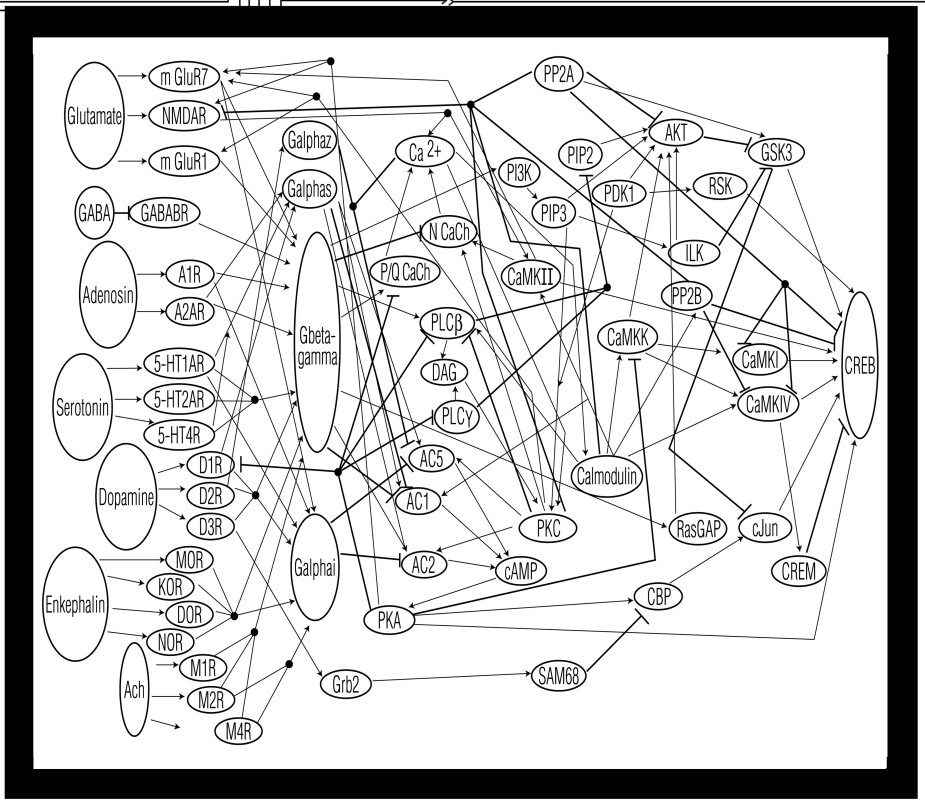

Fault Diagnosis of the Intracellular Microprocessor

Overline: Computational Biology

One sentence summary: An engineering approach reveals the weakest links in cellular signaling networks.

Editor's Summary

Finding Vulnerability
Vulnerability assessment methods, which are commonly used to test digital circuits, were applied to biological signaling networks to identify the molecules that when dysfunctional, would be most likely to disrupt the function of the network. Two signaling well-characterized networks were analyzed (one leading to caspase3 activation and apoptosis and a second leading to activation of p53) and the molecules known to be critical to the response were properly identified. In a third network of neuronal activation of the transcription factor CREB, this analysis lead to the identification of $G\alpha_i$ and the P/Q-type calcium channel, which were then experimentally validated as critical molecules in this network.

Fault Diagnosis Engineering of Digital Circuits Can Identify Vulnerable Molecules in Complex Cellular Pathways

Ali Abdi[1], Mehdi Baradaran Tahoori[2], and Effat S. Emamian[3*†]

[1] Center for Wireless Communications and Signal Processing Research
Department of Electrical and Computer Engineering
New Jersey Institute of Technology
323 King Blvd
Newark, NJ 07102, USA

[2] Department of Electrical and Computer Engineering
Northeastern University
307 Dana Research Building
Boston, MA 02115, USA

[3] Advanced Technologies for Novel Therapeutics (ATNT)
211 Warren Street, Newark, NJ 07103, USA

[†] Work initiated at The Rockefeller University, Box 296
1230 York Avenue
New York, NY 10021, USA

*** Correspondence to: Effat S. Emamian (emame@ATNT-USA.com)**

Abstract

The application of complex system engineering approaches to cell signaling networks should lead to novel understandings and subsequently new treatments for complex disorders. In the area of circuit fault diagnosis engineering, there are various methods to identify the defective or vulnerable components of complex digital electronic circuits. In biological systems, however, knowledge is limited regarding the vulnerability of interconnected signaling pathways to the dysfunction of each specific molecule. By developing proper biologically-driven digital vulnerability assessment methods, the vulnerability of complex signaling networks to the possible dysfunction of each molecule can be determined. To demonstrate the utility of this approach, we analyzed three well-characterized signaling networks-- a cellular network that regulates the activity of caspase-3, a network that regulates the activity of p53, and a central nervous system network that regulates the activity of the transcription factor CREB. We found important differences among the vulnerability values of different molecules. Most of the identified highly vulnerable molecules are functionally related, and known key regulators of these networks. Experimental data confirmed the ability of digital vulnerability assessment to correctly predict key regulators in the CREB network. Because this approach may provide insight into key molecules that contribute to human diseases, it may aid in the identification of critical targets for drug development.

Introduction

Over the past few decades, a large amount of information has been collected regarding the function of individual signaling molecules and many detailed individual molecular mechanisms that regulate cellular function have been identified. Systems biologists have started to integrate these individual interactions and components, to analyze the properties and functions that emerge from these complex biological systems (1).

Each cell in the human body includes many biomolecules, which are interacting with each other through a network of many cellular signaling pathways. Dysfunction of some molecules involved in these pathways may interfere with the efficacy and efficiency of the signal transduction within the network, which can eventually result in a transition from the normal function (physiological condition) to a dysfunctional system (diseased or pathological condition). For some of hereditary human diseases, such as Huntington's disease, neurofibromatosis, and polycystic kidney disease, variations in a single gene cause the pathology. However, for some human diseases, including cancer, as well as some neurodegenerative and psychiatric brain disorders, a single gene does not cause the disorder. Instead, the disease may result from the dysfunction of several molecules in different pathways. In such complex trait disorders, it is not clear which molecules have causative effects, and how much each molecule may contribute to the development of the pathology.

The core idea of this paper is to conceptualize a disorder at the molecular level as a faulty system, in which one or more molecules in the complex intracellular signaling network are dysfunctional. Although genome- and proteome-wide expression analysis of biological systems provides a valuable picture of the “expression levels” of the molecules, it is the “functionality” of each molecule that determines the overall performance of the molecular system. We develop useful molecular fault models, similar to some fault models used in digital circuits (2), to quantify the functionality of different molecules in a network.

Results

There are many similarities between digital electronic circuits and genetic or signaling networks. In a manufacturing facility, a digital circuit is manufactured based on a particular design and is supposed to provide a specific function. However, during the fabrication process, physical defects--faulty transistors, open and short wires, and such--may occur, causing the manufactured circuit not to function according to the design specifications. Testing of digital circuits and systems allows defective manufactured parts to be separated from the nondefective ones, in order to guarantee the production of fault-free products. The test is an assessment of the manufactured circuit, according to a set of criteria. During the lifetime operation of electronic systems, the correct functionality is a key aspect and is typically referred to as reliability.

To determine the most vulnerable molecules in a network of molecules, we take advantage of a class of electronic circuit reliability analysis techniques known as vulnerability assessment methods. Such methods provide numerical values for the vulnerability of the operation of the entire molecular system to the dysfunction of each individual molecule. A high vulnerability for a molecule means that with high probability, the whole signaling network does not operate correctly, if that particular molecule is dysfunctional. Identification of such important molecules, those with high vulnerability values, in signaling networks implicated in disease is a major step towards understanding the molecular basis of complex human diseases. From the drug development perspective, vulnerability assessment provides a set of candidate molecules to target.

To calculate the amount of the vulnerability of a network of interconnected pathways to the dysfunction of each molecule, one needs a model for the network. There are different types of models, such as Boolean, Bayesian, differential equations, algebraic,

and graph theory. We chose the Boolean framework, where each molecule is either active (on) or inactive (off) (3, 4) thus by analogy with digital electronic circuits, the state of a molecule is either 1 or 0, respectively. The Boolean framework and binary logic has been extensively used to explore different characteristics of signaling and genetic networks (3). Through application of digital circuit fault and reliability analysis methods (2) and Boolean models of pathways, we show that the molecular system vulnerability to the dysfunction of each molecule within the system can be computed.

To illustrate this approach, we generated circuit diagrams for a "toy" molecular network (Fig. 1A), which has seven molecules. In Fig. 1A, *A* and *B* are the input nodes (molecules), and *G* is the output node (molecule). Activation and inhibition are shown by lines ended to $\rightarrow$ and $\dashv$, respectively. The activity of each molecule can be shown by a binary value assigned to the name of that molecule. For example, $A = 0$ indicates that *A* is inactive (off), whereas $A = 1$ means that *A* is active (on). To assess the vulnerability of a network, it is necessary to derive a binary logic equation for each molecule of the network. Based on the known physiological mechanisms by which different regulators control the activity of signaling molecules, we propose two rules to derive the logic equations of a molecular network. Rule #1 states that if a molecule has no inhibitory input, then the activation of at least one of its activatory inputs in enough to activate the molecule. Rule #2 states that if a molecule has at least one inhibitory input, then that molecule will be inactive, if at least one of its inhibitory inputs is activated. Moreover, the molecule can be active, only if all the inhibitory inputs are inactive.

Based on the definitions of Boolean OR, AND, and NOT (inversion) , Rule #1 implies the *OR of activatory inputs*; whereas Rule #2 is the *AND of inverted inhibitory*

inputs. When a molecule has both activatory and inhibitory inputs, the two rules are combined, which means the *AND of "inverted inhibitory inputs" with the "OR of activatory inputs"*. Using the above two rules, we derived logic equations for the toy network (Fig. 1B) and based on the five logic equations, we generated a digital electronic circuit for the toy network (Fig. 1C). In digital circuits, there are four types of "gates": AND, OR, BUFFER, and NOT. The following symbols are used to represent these gates: A semi-ellipse represents the AND operation, a bullet-like shape depicts the OR operation, a triangle with a bubble on the right vertex represents the NOT operation (inhibition), a triangle with no bubble is called a BUFFER (activation). The input and output of a BUFFER have the same logic values; if the input is on or off, then the output is on or off, respectively.

To test the validity and feasibility of this approach in cellular signaling networks, we apply this logic to a well-characterized network (Fig. 2A), for which the interactions between the molecules are extensively characterized and experimentally verified (5,6). Janes *et al.* (5) studied the individual and joint effects of the three input nodes, the ligands epidermal growth factor (EGF), insulin, and tumor necrosis factor (TNF), on the activity of the two output nodes caspase3 and forkhead-related transcription factor (FKHR). Their study also showed how the activity of several intracellular intermediate molecules is modulated to regulate the activity of caspase3 and FKHR. The caspase3-FKHR network investigated by Janes *et al*. has 22 nodes, with 27 interactions among them. Using the two rules that we previously defined, we derived a single logic equation for each node in the network (Supplementary Table 1) that includes all the regulatory inputs to each node.

With the logic equations derived for the caspase3-FKHR network, we generated a caspase3-FKHR digital circuit (Fig. 2B) using AND, OR, BUFFER, and NOT gates.

Using the logic equations, the binary logic values of the outputs, FKHR and caspase3, can be determined for any combination of inputs. The resulting “truth table” (Table 1) shows in the first three columns all possible input scenarios and in the last three columns show the calculated outputs, according to the circuit logic equations (Supplementary Table 1). Consistent with the experimental findings (5), digital circuit analysis showed that as long as EGF or insulin is active, caspase3 is inactive, indicating that apoptosis will not occur. However, when both EGF and insulin are inactive and TNF is active, then caspase3 is activated, which can lead to apoptosis. The consistency of the experimental data (5) with the results of the digital circuit analysis validates the biological application of this binary logic engineering approach and suggests that this level of abstraction, the Boolean on/off model, has a coarse predictive power that can be verified experimentally.

To perform the vulnerability assessment for any circuit, the fault model must be specified (2). We chose the class of "stuck-at-0" and "stuck-at-1" fault models, because they seem to be more biologically relevant. To place this model into a biological perspective, consider that each molecule is supposed to change its active or inactive state, according to its input signals. However, if the molecule is “stuck” at a particular state, due to mutations or other structural or functional abnormalities, it can not respond properly to the input signals. The state of such a dysfunctional molecule will not change, even though it may receive stimulatory or inhibitory commands from its surrounding molecules. Thus, a node with the *stuck-at-0* fault means that the logic value of that node (molecule) is always 0 (inactive), irrespective of its inputs. Similarly, a node with the *stuck-at-1* fault implies that the node (molecule) is always 1 (active), and its state does not change if the inputs change.

In the caspase3-FKHR example, if AKT is "stuck-at-1", then according to the logic equation for caspase3 [caspase3=AKT'×(caspase8+JNK1+MK2); (Supplementary Table 1)], caspase3 is 0. This is because 1'=0 and 0×(caspase8+JNK1+MK2)=0. Thus "stuck-at-1" AKT removes the only chance for caspase3 activation, the presence of TNF in the absence of insulin and EGF, and the subsequent apoptosis under normal conditions (Table 1, compare last two columns). This dependence of caspase3 activation and by inference, apoptosis, on the state of AKT is supported by the experimental findings showing that the hyperactivity of AKT (stuck-at-1 in the digital circuit fault analysis) is associated with malignant transformation (7).

The next step in digital circuit fault analysis is calculating the vulnerability of a node. By definition, the vulnerability value of a node is the probability that the system fails (incorrect system output), if that particular node is faulty (dysfunctional). To determine the vulnerability of the network to the dysfunction of each individual molecule, we considered the input signals to be statistically independent, such that each input molecule takes 0 and 1 with the same probability of 0.5. By applying the error probability propagation (EPP) method (8,9) to the caspase3-FKHR circuit (Fig. 2B), we computed the vulnerability values of all the molecules in the caspase3-FKHR network (Table 2).

In this type of analysis, the vulnerabilities of the output nodes are always 1, because if the output nodes are dysfunctional, by definition the network is not functioning correctly. The caspase3-FKHR network shows the highest vulnerability to the dysfunction of AKT, which may be because AKT is the immediate upstream regulator of both the output nodes (Fig. 2A). To clarify this issue, we removed the output node FKHR from the network and recalculated the vulnerabilities of all the nodes (Table 2). Even in this case, AKT still has the highest vulnerability value of all nonoutput molecules, which

implies that AKT plays a critical role in this network. Using the three-input one-output caspase3 network, a biological interpretation for the AKT vulnerability value 0.87 means that if AKT is dysfunctional, then on average, for 87% of all possible ligand binding incidents (input signals), the cell will not correctly regulate the activity of caspase3 (the output node). The computed vulnerabilities (Table 2) are insensitive to the presence or absence of some nodes that have minor effects on the vulnerabilities of the rest of the nodes in the network. For example, removal of p38 from the caspase3-FKHR network, which allows the MKK3 node to activate the MK2 node directly, did not change the vulnerability values of the remaining components. Removal of the NF-κB node or both the p38 node and the NF-κB node also did not change the vulnerability values.

Using the approach of Ma'ayan *et al.* (11), we constructed a p53 cellular network containing numerous intermolecular interactions (Fig. 3A). The p53 network was constructed from pairs of experimentally-verified molecular interactions reported in the literature (see Supplementary Materials for citations). This network was analyzed to test the validity and capability of circuit fault diagnosis engineering to correctly predict the main regulators of p53, which is a tumor suppressor that is a transcriptional activator of several genes that ultimately control cell cycle arrest, cellular senescence, or apoptosis. p53 has been found mutated or functionally inactivated in more than half of all the human cancers (12). The resulting network, called the p53 network, has a total of 49 molecules, with 94 intermolecular interactions. The input nodes are the two ligands insulin and platelet-derived growth factor (PDGF), and the output node is the transcription factor p53. The specific interactions among the molecules of this network are derived from the literature and publicly available databases (see Supplementary Materials). A single specific logic equation for every individual molecule in the p53 network was derived on

the basis of the logic rules (Supplementary Table 2) and these logic equations were used to generate the p53 digital circuit (Supplementary Fig. 2), and the vulnerability values of all the molecules in the network were computed (Table 3).

The p53 network shows the highest vulnerability (more than 0.5) to the dysfunction of phosphatidylinositol-(4,5)-bisphosphate (PIP2), AKT, caspase3, and protein phosphatase 2A (PP2A) (Fig. 3B). Previous studies have experimentally shown that these molecules are known to be the key regulators of p53 (32, 33, 34, 35, 36, 37, 38). Thus, the analysis predicts that if any one of these molecules is dysfunctional, out of 100 incidents of ligand binding, over 50 times p53 will not function properly. The distribution of the vulnerability values of the molecules is nonuniform (Fig. 3C). There were four highly vulnerable nodes (>0.5), six moderately vulnerable nodes (values between 0.1 and 0.5), and a majority of the nodes (38 out of the 49) exhibited very low vulnerability values (less than 0.1) (Fig. 3B).

The four molecules that had the highest vulnerability values in the p53 network are known to be key regulators of the cellular functions for which p53 is responsible. For AKT and caspase3, there is clear evidence that these two molecules play crucial roles in regulating a number of p53-regulated functions, such as cell survival and apoptosis (12,13). More importantly, there is experimental evidence supporting a key role for AKT in proper activation of p53 (32, 33, 34). Although PIP2 have not been directly connected to p53, it is a regulator of AKT and thus this connection to AKT may explain its high vulnerability value. The experimental evidence that PP2A and caspase3 plays a major role in regulating p53 activity comes from (35, 36, 37). Thus, molecules diagnosed as faulty by this approach are experimentally known to contribute to failure of the system

and cause pathology in humans. This can confirm the reliability of this novel methodology.

We also constructed a complex neuronal network, following the same approach of Ma'ayan *et al.* (11). The output node is the transcription factor CREB (cAMP responsive element binding protein) and the input nodes are seven major ligands in nervous system--glutamate, dopamine, GABA, serotonin, ACh, adenosine, and enkephalin. The CREB network (Fig. 4A) is comprised of 64 molecules and 152 intermolecular interactions (see Supplementary Materials). The logic equations for the CREB network (Supplementary Table 3) were derived using Rule #1 and Rule #2, and the corresponding digital electronic circuit, was constructed (See Supplementary Fig. 4). Calculation of the vulnerabilities of all the molecules (Table 4) once again revealed a nonuniform distribution (Fig. 4C). Indeed, dysfunctional in 41 molecules out of 64 would not contribute to the failure of CREB circuit (vulnerability values less than 0.1).

The molecules with a vulnerability of more than 0.5, which indicates that their dysfunction can result in the failure of CREB function, are calmodulin, calcium, cAMP, $G\alpha_i$ (abbreviated Galphai in the network diagram), adenlyate cyclase 1 (AC1), AC2, AC5, protein kinase A (PKA), P/Q-type calcium channel (abbreviated P/QCaCh in the network diagram), and PP2A (Table 4 and Fig. 4B). These molecules can be grouped into elements of the cAMP-dependent signaling (cAMP, $G\alpha_i$, PKA, and the AC isoforms) and elements of calcium signaling (calcium, calmodulin, and P/Q-type calcium channels). Furthermore, the distribution of the vulnerability values in the CREB network is highly

non-uniform (Fig. 4C). Fig. 4B shows the molecules with the highest vulnerability values in the CREB network are functionally related molecules, and some of them are already known as main physiological regulators of CREB function. Indeed the name CREB is based on the identification of the protein as a cAMP responsive element binding protein. This engineering analysis has identified cAMP and the molecules directly related to cAMP function, such as AC1, AC2, AC5, and PKA, as the most critical molecules for the regulation of CREB. The crucial role of PKA in the regulation of CREB is well known (14). Important functions of the cognitive and executive human brain, such as learning and memory, are directly regulated by cAMP-dependent CREB functions (14). In pathological terms, direct evidence for deregulation of PKA signaling has been reported in human disorders manifested by memory dysfunction, such as Alzheimer Disease (18) or schizophrenia (19, 31). Vulnerability assessment of the CREB circuit has also identified some elements of calcium signaling as playing a major role in the function of CREB. This observation is also physiologically and pathologically relevant and consistent with experimental data (20). Furthermore, several pathological conditions associated with memory dysfunction can arise from deregulation of calcium-dependent signaling (21-23). Although it is not yet clear how CREB is involved in the pathogenesis of these disorders, the physiological role of CREB in neuronal mechanisms underlying the memory function of mammalian brain has been known for many years (14).

Because many of the identified molecules are already experimentally known regulator of CREB, we provide experimental evidence for only two, $G\alpha_i$ and P/Q-type calcium channels. We altered the activity or abundance of endogenous P/Q-type calcium channels and $G\alpha_i$ in primary cortical neurons from rats and then assayed for the changes in endogenous CREB activity or abundance (see Methods). We used primary neuronal

culture as a model system because it has the most similar CREB signaling network to the *in vivo* signaling networks of the mammalian brain.

Short-term (2.5 h) treatment of primary neurons with the selective P/Q-type calcium channel blocker, ω-Agatoxin IVA, increased the phosphorylation of CREB at Ser^{133}, without changing the total abundance of CREB (Fig. 5A). In contrast, long-term (12 h) treatment decreased the phosphorylation of CREB at Ser^{133}, as well as decreased the abundance of CREB (Fig. 5A). Furthermore, we targeted the expression of P/Q-type calcium channels with three unique adenoviral shRNA constructs and measured their effect on the endogenous total protein and the phosphorylation levels of CREB at Ser^{133}. Three unique adenoviral shRNA expression vectors (CACNA1A V1, V2, and V3), which target the expression of transcript variants 1 and 2 of the alpha 1A subunit of P/Q-type calcium channels were used to knockdown the expression of the channels in neurons. The V2 vector caused a substantial decrease in the abundance of P/Q-type calcium channels, the V1 vector caused a smaller decrease in the abundance, and V3 did not affect the abundance of the channel in primary neurons. We observed a decrease in the abundance of CREB and in the proportion of Ser^{133} phosphorylated CREB in cells with the V2 vector. However, the V3 vector, which did not alter P/Q-type calcium channel abundance, did not affect the abundance or phosphorylation of CREB. These experiments show that the activity or abundance of P/Q-type calcium channels can affect both the abundance and phosphorylation state of CREB. This observation is consistent with the findings of Sutton *et al.* (15), which shows exogenous expression of P/Q-type calcium channels can induce transcription of specific genes related to the synaptic function. Whether P/Q-type calcium channels are altering calcium signaling to affect CREB activity or whether they are functioning through a nonconducting mechanism, similar to

that described for other types calcium channels (L and N type) (16), remains to be determined. It is also an open question as to why there are opposing effects of short-term and long-term blockage of P/Q-type calcium channel activity on CREB phosphorylation. A possible biological explanation for the different response between the short and long term treatments is related to the compensatory mechanisms that re-regulate the initial cellular response. The existing feedbacks in the circuit may explain the role of compensatory mechanisms that occur within different time intervals in biological systems. More detailed studies are needed to precisely address the differences among short and long term responses.

To verify the importance of $G\alpha_i$ in the regulation of CREB we inhibited $G\alpha_i$ with pertussis toxin (17) (see Methods) and found an increase in the abundance CREB and an increase in Ser^{133} phosphorylation. In contrast, activation of $G\alpha_i$ by MAS-7, an active mastoparan analog that stimulates $G\alpha_i$ (17), caused a decrease in the abundance of CREB and a decrease in Ser^{133} phosphorylation (Fig. 5C). The decrease in abundance of CREB, along with the decrease in Ser^{133} phosphorylation, is consistent with an overall decrease in the activity of CREB, as phosphorylation of CREB at Ser^{133} is required for activity (14). Thus, the active/inactive Boolean framework used for modeling and vulnerability analysis lead to discovery of both regulation by changes in abundance and phosphorylation state. These experiments demonstrate the ability of the fault diagnosis engineering approach to correctly identify key regulators of signaling pathways.

With the primary neuronal cultures, we tested the ability of the constructed Boolean network to correctly predict the output activity, following an increase in the concentration

of each input molecules. More specifically, we experimentally verified the accuracy of the following table, obtained using the logic equations of the CREB network (Supplementary table 3). This table shows the binary logic values of the output CREB, when different inputs are applied to the circuit. The first five columns include the input scenarios, whereas the last three columns are computed by simulating the circuit logic equations in ModelSim®, a simulation and debug software tool for digital circuits.

Input ligands					Output		
Serotonin	Glutamate	Dopamine	GABA	Adenosine	CREB (PKA normal)	CREB (PKA stuck-at-1)	CREB (PKA stuck-at-0)
1	0	0	0	0	1	0	0
0	1	0	0	0	0	0	0
0	0	1	0	0	0	0	0
0	0	0	1	0	0	0	0
0	0	0	0	1	0	0	0

According to this table, serotonin is the only input that activates CREB, when PKA is functional. To verify this prediction experimentally, we treated primary neurons that express these receptors (39) with 10 μM activatory concentration of serotonin (40), glutamate (42), dopamine(41), GABA(43), and adenosine (44) for 15 minutes then measured the activity of CREB by monitoring Ser^{133} phosphorylation (14). As shown in Fig. 5D, treatment with serotonin had the most robust effect on the activity of CREB, stimulating phosphorylation to a similar extent as did the PKA activator forskolin. However, exposure of the neurons to the other ligand failed to robustly activate CREB (Fig. 5D). This is consistent with the output predicted by the logic equations and listed in the above table: Serotonin should be the most effective activator of CREB. Previous studies have also reported that serotonin can induce Ser^{133} CREB phosphorylation (26,

40), thus the engineering model not only correctly predicts this effect of serotonin, but also shows the specificity of serotonin's effect, compared to the other ligands.

We also tried to verify the biological relevance of the stuck-at-1 and stuck-at-0 fault models, which are included in the last two columns of the above table. We tested the effect of serotonin on the activity of CREB when PKA, a highly vulnerable molecule in this network, is either activated (stuck-at-1) or inhibited (stuck-at-0), by forskolin or H-89, respectively. When PKA is stuck-at-1 or 0, the model predicts that serotonin should no longer activate CREB (See the last two columns of the above above). To verify this experimentally, we treated primary neurons with serotonin in the presence or absence of either forskolin or H-89 (Fig. 5E). Whereas individual treatments with serotonin or forskolin activate CREB, treatment with serotonin following activation of PKA by forskolin attenuated the effect of forskolin on the activity of CREB, as compared to treatment with serotonin only. This is while the general expectation in biology is that addition of two activators of CREB, i.e., serotonin and forskolin, should enhance the activatory effect. Thus, when the highly vulnerable molecule PKA is stuck-at-1, the network output is not correctly regulated by the input. Inhibition of PKA by H-89 also prevents serotonin from stimulating the activity of CREB (Fig. 5E). Immunofluorescent analysis of CREB phosphorylation in primary neuron cultures exposed to vehicle, forskolin, or serotonin individually, or to serotonin following treatment with forskolin, was consistent with the results obtained by Western blotting for CREB phosphorylation. The cells were triple labeled with antibodies against Ser^{133} CREB (as a measure of CREB activity), Map-2 (as a marker that specifically labels neurons), and DRAQ-5 (as a nuclear marker that stains the nucleus of neuronal and nonneuronal cells in primary culture). Treatment of the neuronal primary cultures with forskolin increased the activity

of CREB in both neuronal and non-neuronal (glial) cells in primary culture. However, treatment with serotonin only increased the activity of CREB in neurons, not in the nonneuronal cells. This specific activation in the neuronal cell population by serotonin was expected, because neurons have receptors for serotonin whereas the nonneuronal cells in the culture do not. Consistent with the Western blot data (Fig. 5E), the effect of serotonin on the activity of CREB in neurons is attenuated, when serotonin was added after treatment with forskolin. These two experiments suggest that dysfunction of the network output occurs when PKA is stuck in either an active or inactive state. Thus, the data support the prediction of the model that serotonin fails to activate CREB when PKA is faulty, which is entirely consistent with PKA having a high vulnerability value in the network.

Discussion

Taken together, our experimental data indicates that fault diagnosis engineering can identify new critical regulators, and also correctly predict previously known regulators of the output molecules. Furthermore, we have provided experimental evidence that a reconstructed Boolean network can correctly predict the activity of output molecules, based of the activity levels of input signals. Finally, our experimental data supports the theoretical finding of the proposed fault diagnosis approach, specifically the experiments confirm that for proper propagation of the input signals to regulate the activity of output molecules, the normal function and activity level of highly vulnerable molecules are necessary. When these highly vulnerable molecules become faulty, stuck-at-1 or 0, the

interconnected pathways can not correctly propagate the signals from input to the output, and the molecular network does not function properly.

Boolean modeling has certain applications and it is not the claim of the paper that it can be used to precisely model all characteristics of signaling networks. The usefulness of Boolean modeling depends on the goal of the study. In the present study, Boolean framework provides a model that captures those essential characteristics of a molecular network that we needed, to determine the vulnerability of the network function to the dysfunction of each molecule. Boolean approach has provided biologically-relevant results in the paper, consistent with both the experimental findings of other research groups and the experiments of the paper. The proposed approach can be extended in several directions, to broaden its scope. For example, two rules were introduced in the paper, to build digital circuit equivalents of large signaling molecular networks. When looking at each individual molecule in the networks we studied, the two rules were found to be sufficient. Verification of the computational results with experiments further validated the approach. However, it is possible that the activation or inhibition of a particular molecule may differ from what considered in the two rules. Examples may include molecules that need sequential phosphorylation to become activated, or competitive inhibition mechanisms of some molecules. In such scenarios, certainly an appropriate mixture of AND/OR/NOT operations can be used, to properly model the activity of the molecule in terms of its inputs.

There are a number of different modeling approaches such as differential equations, Boolean models, graphs, Bayesian models, etc. We chose the Boolean modeling framework as it provides a picture of cell signaling which was sufficient for the goal we had, as confirmed by the experimental results of the paper. It also has a certain prediction

power which was validated by experiments as well. When it comes to finding important molecules, one may think of graph theory and sensitivity analysis. Graph theoretical approaches make conclusions based on the topology and connections that exist among the nodes of a graph that represents a molecular network. Based on the existing literature and to the best of our knowledge, since these assertions are not compared with experiments, we cannot comment on their usefulness regarding the identification of critical molecules.

Sensitivity analysis methods are typically used in conjunction with differential equation models of molecular networks, to determine the sensitivity of the concentration levels to the variations of kinetic parameters and rate constants (30). So, to implement such sensitivity analysis methods in large signaling networks, the nominal values of a large number of kinetic parameters and concentration levels need to be determined first. The proposed Boolean vulnerability assessment framework, however, does not use these parameters and can identify vulnerable molecules using less detailed information. Experiments are conducted and reported in the paper, to verify the usefulness of the proposed approach.

In summary, this paper takes advantage of the concepts of electronic circuit fault diagnosis engineering, to identify the vulnerable molecules that play crucial roles in the dysfunction of molecular networks. The vulnerable molecules identified in caspase-3, p53, and CREB signaling networks are functionally related sets of molecules, with physiological and pathological relevance to the specific function of each network. This indicates the usefulness of the proposed approach. Application of this technique can improve the physiological understanding of the functionality of biological systems,

identify key regulatory components, and potentially identify important targets for drug discovery.

Materials and Methods

Constructing the networks

For the caspase3-FKHR network, we used the experimentally-verified networks of Janes *et al.* (5,6). For the p53 and CREB networks, we employed the approach of Ma'ayan *et al.* (11), as follows. First the inputs nodes (ligands) and the output node (transcription factor) of interest were specified, as well as the intermediate molecules that transmit the input signals to the output. Then the type of the interactions among the molecules (activatory or inhibitory) were determined, using the existing literature and databases (See Supplementary Materials for details).

Identification of the feedback paths

We used the depth-first search (DFS) algorithm (10) to identify the feedback paths. This step is done after a digital circuit is created. First the digital circuit model is converted into a graph model. Each node in the digital circuit is modeled as a node in the corresponding graph and connections between the logic gates are modeled as edges in the graph. The DFS traversal is applied to the graph model to identify the feedback loops (10). This traversal visits all nodes of the graph one by one in the topological order by traversing the paths in the graph. Whenever a node is revisited (i.e., visited twice) in a path, it indicates the existence of a loop in the graph. Then, the loop is broken by

removing the edge and replacing the corresponding connection in the digital circuit with a flip-flop. A flip-flop is a one-bit digital logic memory unit. This process is repeated until no further loop can be identified, i.e., DFS traversal of the modified graph can be concluded without revisiting any node.

Vulnerability analysis of the logic circuits

We present a methodology for reliability analysis (vulnerability analysis) of logic circuits and its application to biological signaling networks to calculate the vulnerability values for the molecules in the network.

We extract the error propagation probability (EPP) of the internal nodes, which is the probability that an erroneous value on that node propagates from the error site to system outputs and results in an observable error in the system. We developed an EPP computation approach, which improves the runtime of previous EPP methods by several orders of magnitude. The presented approach uses the signal probabilities (SP) of all nodes in the combinational part and then computes EPPs based on the topological structure of the logic circuit. The signal probability (SP) of a line *l* indicates the probability of *l* having logic value 1 (24). Experiments on benchmark circuits and comparison of the results with the fault injection method based on random simulation show the effectiveness and the accuracy of the presented approach (9).

We first extract the structural paths from the error sites to all reachable primary outputs and then traverse these paths to compute the propagation probability of the erroneous value to the reachable primary outputs or to the reachable flip-flops. Based on the error site, we categorize nets and gates in the circuit as follows. An *on-path* signal is a net on a path from the error site to a reachable output. Also, an *on-path gate* is defined as

the gate with at least one on-path input. Finally, an *off-path* signal is a net that is not on-path and is an input of an on-path gate (See Supplementary Fig. 5).

For error propagation probability calculation, as we traverse the paths, we use signal probability for off-path signals and use our propagation rules for on-path signals. SP calculation and estimation techniques have been presented previously (25). The problem statement can be described as follows:

Given the failure probability in node n_i, calculate the probability of the propagation of this error to Primary Outputs (POs) or Flip-Flops (FFs) (that is, system failure).

Errors can be directly propagated to a primary output and cause a system failure at the same clock cycle, or they can be propagated to flip-flops repeatedly, and finally manifest as errors at a primary output several clock cycles later.

First, consider a simple case when there is only one path from the error site to an output. As we traverse this path gate by gate, the error propagation probability from an on-path input of a gate to its output depends on the type of the gate and the signal probability of other off-path signals. In the example shown in Supplementary Fig. 6, the error propagation probability to the output of the gate C (AND gate) is the product of the probability of the output of gate A being 1 and the error probability at the PI ($1\times0.2=0.2$). Similarly, EPP at the output of the gate D (OR gate) is calculated as $0.2\times(1-SP_B) = 0.2\times0.7=0.14$.

In the general case in which *reconvergent paths* (one signal directly or indirectly drives more than one input of a logic gate) might exist, the propagation probability from the error site to the output of the reconvergent gate depends on not only the type of the gate and the signal probabilities of the off-path signals, but also the polarities of the

propagated error on the on-path signals. In the presence of errors, the status of each signal can be expressed with four values:

- 0: no error is propagated to this signal line and the signal has an error-free value of 0.
- 1: no error is propagated to this signal line and it has logic value of 1.
- a: the signal has an erroneous value with the same polarity as the original erroneous value at the error site (denoted by a).
- $\bar{a}$: the signal has an erroneous value, but the erroneous value has an opposite polarity compared to the erroneous value at the error site (denoted by $\bar{a}$).

Based on this four-value logic, we can redefine propagation rules for each logic gate. These probabilities, denoted by $P_a(U_i)$, $P_{\bar{a}}(U_i)$, $P_1(U_i)$, and $P_0(U_i)$, are explained as follows:

- $P_a(U_i)$ and $P_{\bar{a}}(U_i)$ are defined as the probability of the output of node U_i being a and $\bar{a}$, respectively. In other words, $P_a(U_i)$ is the probability that the erroneous value is propagated from the error site to U_i with an even number of inversions, whereas $P_{\bar{a}}(U_i)$ is the similar propagation probability with an odd number of inversions.
- $P_1(U_i)$ and $P_0(U_i)$ are defined as the probability of the output of node U_i being 1 and 0, respectively. In these cases, the error is blocked and not propagated.

Note that for on-path signals, $P_a(U_i) + P_{\bar{a}}(U_i) + P_1(U_i) + P_0(U_i) = 1$, and for off-path signals $P_1(U_j) + P_0(U_j) = 1$. Because we have considered the polarity of error effect propagation, this will take care of reconvergent points. The error propagation calculation rules for elementary gates are shown in Supplementary Table 4. To illustrate how to employ the propagation rules for reconvergent paths, consider the example shown in Supplementary Fig. 7. In this example, the error propagation probability from the output of gate A to PO is calculated. Assume that the gate A becomes erroneous. So, initially,

we set $P_a(A)=1$, $P_{\bar{a}}(A)=0$, $P_1(A)=0$, and $P_0(A)=0$. Then, we propagate these probabilities through gates D, E, and H. As an example, we do the following steps to compute the error propagation probability of the erroneous value to the output of gate H.

$\mathbf{P_0(H)} = P_0(C)\times P_0(D)\times P_0(G) = 0.7\times 0.8\times 0.3 = 0.168$

$\mathbf{P_a(H)} = (P_0(C) + P_a(C)) \times (P_0(D) + P_a(D)) \times (P_0(G) + P_a(G))$

$- P_0(H) = (0.7)\times(0.2+0.8)\times(0.3) - 0.168 = 0.042$

$\mathbf{P_{\bar{a}}(H)} = (P_0(C) + P_{\bar{a}}(C)) \times (P_0(D) + P_{\bar{a}}(D)) \times (P_0(G) + P_{\bar{a}}(G))$

$- P_0(H) = (0.7)\times(0.8)\times(0.7+0.3) - 0.168 = 0.392$

$\mathbf{P_1(H)} = 1 - (0.168 + 0.042 + 0.392) = 0.398$

➔ $\mathbf{P(H)} = 0.042(a) + 0.392(\bar{a}) + 0.168(0) + 0.398(1)$

Finally, the EPP of gate A to outputs can be computed as:

$EPP_{A\rightarrow PO} = [P_a(H)+P_{\bar{a}}(H)] = (0.042 + 0.392) = 0.434$

In general, the following algorithm shows how we can extract and then traverse all paths from a given error site to all reachable outputs and how we apply the propagation probability rules as we traverse the paths.

The Main Algorithm

For every node, n_i, do:

1) **Path Construction**: Extract all on-path signals (and gates) from n_i to every reachable primary output PO_j and/or flip-flop FF_k. This is achieved using the forward Depth-First Search (DFS) algorithms (10).
2) **Ordering**: Prioritize signals on these paths based on their distance level using the *topological sorting* algorithm (10). Topological sort of a directed acyclic graph is an ordered list of the vertices such that if there is an edge (u, v) in the graph, then u appears before v in the list.

3) **Propagation Probabilities Computation**: Traverse the paths in the topological order and apply propagation rules to compute the probability for each on-path node based on propagation probability rules (Supplementary Table 4).

Using the above formulation, error propagation probabilities from an arbitrary error site to any flip-flop, primary output, or both can be computed in just one pass starting from the error site to reachable output. As a result, the complexity of this approach is linear to the size of the circuit (number of logic gates). In other words, the exponential path enumeration problem is not observed in this algorithm. After computing the EPP of each node to all outputs, the overall EPP of an arbitrary node A to all primary outputs at the first clock cycle can be computed as:

$$EPP_{c=1}(A) = 1 - \prod_{i=1}^{k} 1 - EPP_{A \to PO_i}$$

where k is the number of primary outputs. Note that $EPP_{c=1}(A)$ computes the EPP of node A at the first clock cycle. The transient error, however, can be captured in flip-flops and propagated to primary outputs in the next clock cycles. To compute EPP of a node in the next clock cycles ($c > 1$), the same error propagation rules can be repeated in the next cycles. Note that in multiple cycle simulations ($c > 1$), the transient error disappears from the original error site. In this case, flip-flops are considered as possible error sites. Using the error propagation rules $EPP_{c=2}(A)$, $EPP_{c=3}(A)$, $EPP_{c=4}(A)$ are computed accordingly. Our experiments show that $EPP_{c=x}(A)$ for $x > 4$ becomes very close to 0 such that we can ignore these probability values without sacrificing any accuracy. Finally, we compute the overall EPP of a node A according to the following equation:

$$
\begin{aligned}
EPP(A) = {} & EPP_{c=1}(A) + \\
& \left(1 - EPP_{c=1}(A)\right) \times EPP_{c=2}(A) + \\
& \left(1 - EPP_{c=1}(A)\right) \times \left(1 - EPP_{c=2}(A)\right) \times EPP_{c=3}(A) + \\
& \left(1 - EPP_{c=1}(A)\right) \times \left(1 - EPP_{c=2}(A)\right) \times \left(1 - EPP_{c=3}(A)\right) \times EPP_{c=4}(A)
\end{aligned}
$$

In order to run our vulnerability analysis methodology for the biological circuits of interest, we first need to convert their set of Boolean equations (Supplementary Table 1, Supplementary Table 2 and Supplementary Table 3) into sequential circuits, without any combinational feedback (the original set of equations contain combinational feedbacks). For this purpose, the feedback paths of these circuits are extracted using the DFS algorithm (10). Then, appropriate flip-flops are inserted at each feedback path, identified by backward edges in the DFS, to convert the original circuits to sequential circuits (Supplementary Fig. 2 & 4). Because the Boolean equations of Supplementary Table 1 do not have any combinational feedback, no flip-flop is inserted in the corresponding combinational circuit (Fig. 2B). Finally, the vulnerability analysis algorithm is applied to the circuits, to extract the SP and EPP values for all the nodes.

Developing the EPP method for the toy molecular network

As an example, we explain the EPP method for the digital electronic circuit (Fig. 1C) of the toy molecular network (Fig. 1A). First, we need to obtain the signal probabilities (SP) of all nodes. Staring with input signal probabilities of 0.5, this yields the following:

SP(A) = 0.5, SP(B) = 0.5

SP(D) = SP(A) = 0.5

SP(C) = 1 – SP(B) = 0.5

SP(E) = 1 – [(1 – SP(B) × (1 – SP(D)] = 0.75

SP(C+D) = 1 – [(1 – SP(C) × (1 – SP(D)] = 0.75

$SP(E') = 1 - SP(E) = 0.25$

$SP(F) = SP(E') \times SP(C+D) = 0.185$

$SP(G) = 1 - [(1 - SP(F) \times (1 - SP(E)] = 0.796875$

Once we have the signal probability values of all nodes in the circuit, we can apply the error propagation probability rules (4) to the logic gates in the circuit, starting from input towards the output, to obtain EPP values for the output.

The topological order of this circuit is as follows:

A, B : level 0

C, D : level 1

E : level 2

F : level 3

G : level 4

Given an error in input A (dysfunction in the corresponding molecule), the probability that this error affects the output (causing the system to fail) is obtained as follows:

Since A is erroneous, $P_a(A)=1$, $P_{\bar{a}}(A)=0$, $P_1(A)=0$, and $P_0(A)=0$.

$P_a(B)=0$, $P_{\bar{a}}(B)=0$, $P_1(B)=0.5$, $P_0(B)=0.5$

$P_a(C)=0$, $P_{\bar{a}}(C)=0$, $P_1(C)=0.5$, $P_0(C)=0.5$

$P_a(D) = P_a(A)=1$, $P_{\bar{a}}(D) = P_{\bar{a}}(A)=0$, $P_1(D) = P_1(A)=0$, $P_0(D) = P_0(A)=0$

$P_0(E)= P_0(B)\times P_0(D) = 0$

$P_a(E)=[0.5\times1] - 0 = 0.5$,

$P_{\bar{a}}(E)=0$,

$P_1(E)=1 - (0+0.5+0) = 0.5$,

$P_a(E')=0$, $P_{\bar{a}}(E')=0.5$, $P_1(E')=0$, $P_0(E')=0.5$

$P_0(C+D)= P_0(C)\times P_0(D) = 0$

$P_a(C+D)=[0.5\times1] - 0 = 0.5$,

$P_{\bar{a}}(C+D)=0$,

$P_1(C+D)=1 - (0+0.5+0) = 0.5$,

$P_1(F)= P_1(C+D)\times P_1(E') = 0$,

$P_a(F)=[0\times1] - 0 = 0$,

$P_{\bar{a}}(F)= [0.5\times0.5] - 0 = 0.25$,

$P_0(F)=1 - (0+0+0.25) = 0.75$,

$P_0(G)= P_0(E)\times P_0(F) = 0$

$P_a(G)=[0.5\times0.75] - 0 = 0.375$,

$P_{\bar{a}}(G)=0$,

$P_1(G)=1 - (0+0.375+0) = 0.625$.

The probability of error propagation from A to output G is calculated as

$EPP(A\rightarrow G) = P_a(G)+ P_{\bar{a}}(G) = 0.375$.

Similarly, the error propagation probabilities from all other nodes to the output can be computed and the signals can be ranked based on their EPPs.

Primary cortical culture

Primary cortical cultures were prepared from brains of embryonic day 17 to 18 Sprague-Dawley rats (Charles River). After trituration of cortical sections with a glass pipette, 2 to 4×10^5 neurons were plated on a coverslip (diameter: 12 mm) precoated with poly d-lysine (BD Biocoat). For biochemical analysis, primary cortical cells were plated in 35 mm dishes precoated with poly d-lysine (~3×10^6 neurons/dish). Neurons were grown in

NEUROBASAL Medium supplemented with 0.5 mM L-glutamine, B27 (2%), and N2 (1%) supplements.

Protein extraction, and immunoblot analysis

Primary neurons were cultured as described. Cells were homogenized in ice cold lysate buffer (0.25 M Tris, pH 7.5) containing protease inhibitors (Protease Inhibitor Cocktail tablets, Boehringer Mannheim) and phosphatase inhibitors (Phosphatase Inhibitor Cocktails I & II, Sigma) and lysed through three cycles of freezing (in liquid nitrogen) and thawing (in 37ºC water bath). Protein concentration was measured by Bio-Rad's protein assay and spectrometry at 595 ºA. Equal amounts of total protein were loaded on 4–12% gradient Bis-Tris gels, separated using the NuPAGE system (Invitrogen) and transferred onto nitrocellulose membrane. The membrane was probed with primary and secondary antibodies and signals were detected by chemilluminescence followed by autoradiography. The following antibodies were used: anti-CREB antibody (Cell Signaling, 1:1000), anti-phospho Ser^{133} CREB antibody (Cell Signaling, 1:1000), anti P/Q type calcium channel antibody (Chemicon, 1:1000), and anti-actin antibody (Sigma, 1:1000).

Immunofluorescent studies

Cortical neurons were grown on coverslips, fixed for 10 min in PBS plus 3.7% formaldehyde, and permeabilized for 2 min with cold acetone. Coverslips were coated with 100 µl of primary antibody diluted in PBS (anti Phospho Ser^{133} CREB, Cell Signaling, 1:200, anti Map-2 antibody, Upstate Biotechnology, 1:250). Coverslips

washed three times and labeled with Alexa 568 anti-rabbit antibody (1:500), Alexa 488 anti-mouse antibody (1:500), and the nuclear marker DRAQ-5 (1:10,000).

Analysis of CREB regulation by P/Q-type calcium channels or $G\alpha_i$

Primary cortical neurons were cultured as described. We followed the methods of Dolmetsch et al.(27) to analyze the effect of calcium channel blockers on CREB activity. We characterized the signaling properties of the endogenous P/Q-type calcium channels by monitoring the endogenous activity and total protein levels of CREB. In order to minimize the effect of other elements of calcium or G protein signaling following neuronal depolarization, all experiments were performed without depolarizing the neurons. Previous time-course studies have shown that short-term Ser^{133} phosphorylation of CREB are transient events and prolonged Ser^{133} phoaphorylation (more than 40 minutes) is required for transcriptional activity (27, 28, 29).. Therefore, in these experiments we analyzed the endogenous Ser^{133} phosphorylation and total CREB protein abundance following at least 2 hours treatment with agonist or antagonists of P/Q-type calcium channels and 2 hours treatment with agonist or antagonist of $G\alpha_i$. ω-Agatoxin IVA (Calbiochem), pertussis toxin (Sigma), and Mas-7 (Calbiochem) were dissolved in the appropriate vehicle and added to the medium. Following the treatment, cortical neurons were harvested, lysed, and subjected to Western blot analysis as described.

Adenoviral gene knockdown

We used AdenoSilence^{TM} RNAi viral vector kit (Millipore, Cat# GAL10021) to target the expression of P/Q-type calcium channels in primary neuronal cultures. This kit

consisted of three unique adenoviral shRNA constructs targeting the transcript variants 1 and 2 of the alpha 1A subunit of P/Q-type calcium channels (CACNA1A). Following the kit instruction, 60×10^6 VPU (Viral Particle Unit) from the crude virus of each construct was added to 50 ul of complete medium and added to 35-mm dishes of primary neuronal cultures. Cells were harvested 48 hours after viral transduction, protein was extracted, and the lysates were subject to Western blot analysis.

Supplementary Materials

References

1. Alberghina, L., & Westerhoff, H. V. (Eds.) *Systems Biology*. Springer (2005).
2. Bushnell, M. L. & Agarwal, V.D. *Essentials of Electronic Testing for Digital, Memory and Mixed-Signal VLSI Circuits*. Kluwer Academic Press (2000).
3. Kauffman, S. A. *The Origins of Order: Self-Organization and Selection in Evolution*. Oxford University Press (1993).

4. Helikar, T., Konvalina, J., Heidel, J. & Rogers, J. A. Emergent decision-making in biological signal transduction networks. Proc. Natl. Acad. Sci. U.S.A. 105: 1913-1918 (2008).

5. Janes, K. A. et al. The response of human epithelial cells to TNF involves an inducible autocrine cascade. *Cell* **124:** 1225-1239 (2006).

6. Janes, K. A. et al. A high-throughput quantitative multiplex kinase assay for monitoring information flow in signaling networks: Application to sepsis-apoptosis. *Mol. Cell. Proteomics* **2:** 463-473 (2003).

7. Luo, J., Manning, B. D. & Cantley, L. C. Targeting the PI3K-Akt pathway in human cancer: Rationale and promise. *Cancer Cell* **4:** 257-262 (2003).

8. Asadi, H., & Tahoori, M. B. Soft error modeling and protection for sequential elements. *Proc. IEEE International Symposium on Defect and Fault Tolerance of VLSI* 463-474 (2005).

9. Asadi, H., & Tahoori, M. B. An analytical approach for soft error rate estimation in digital circuits. *Proc. IEEE International Conference on Circuits and Systems* 2991-2994 (2005).

10. Cormen, T. H., Leiserson, C. L., Rivest, R. L., & Stein, C. *Introduction to Algorithms*. 2nd ed. MIT Press & McGraw-Hill (2001).

11. Ma'ayan, A. et al. Formation of regulatory patterns during signal propagation in a mammalian cellular network. *Science* **309:** 1078-1083 (2005).

12. Levine, A. J., Hu, W. & Feng, Z. The p53 pathway: What questions remain to be explored? *Cell Death Differ.* **13:** 1027-1036 (2006).

13. Brazil, D. P., Yang, Z. Z., & Hemmings, B. A. Advances in protein kinase B signaling: AKTion on multiple fronts. *Trends Biochem. Sci.* **29:** 233-242 (2004).

14. Lonze, B. E. & Ginty, D. D. Function and regulation of CREB family transcription factors in the nervous system. *Neuron* **35:** 605-623 (2002).

15. Sutton, K. G., McRory, J. E., Guthrie, H., Murphy, T. H. & Snutch, T. P. P/Q-type calcium channels mediate the activity-dependent feedback of syntaxin-1A. *Nature* **401:** 800-804 (1999).

16. Ikeda, S. R. Signal transduction: Calcium channels - Link locally, act globally. *Science* **294:** 318-319 (2001).

17. Jena, B. P. et al. Gi regulation of secretory vesicle swelling examined by atomic force microscopy. *Proc. Natl. Acad. Sci. USA* **94:** 13317-13322 (1997).

18. Jicha, G. A. et al. cAMP-dependent protein kinase phosphorylations on tau in Alzheimer's disease. *J Neurosci.* **19:** 7486-7494 (1999).

19. Millar, J. K. et al. DISC1 and PDE4B are interacting genetic factors in schizophrenia that regulate cAMP signaling. *Science* **310:** 1187-1191 (2005).

20. West, A. E. et al. Calcium regulation of neuronal gene expression. *Proc. Natl. Acad. Sci. USA* **98:** 11024-1031 (2001).

21. Lidow, M. S. Calcium signaling dysfunction in schizophrenia: a unifying approach. *Brain Res Rev.* **43:** 70-84 (2003).

22. Tu, H. et al. Presenilins form ER Ca2+ leak channels, a function disrupted by familial Alzheimer's disease-linked mutations. *Cell* **126:** 981-993 (2006).

23. Hans, M. et al. Functional consequences of mutations in the human alpha1A calcium channel subunit linked to familial hemiplegic migraine. *J Neurosci.* **19:** 1610-1619 (1999).

24. Parker, K. P., & McCluskey, .E. J. Probabilistic treatment of general combinational networks. *IEEE Trans. Computers* **24:** 668-670 (1975).

25. Kodavarti, R., & Ross, D. E. Signal probability calculation using partial functional manipulation. *Proc. IEEE VLSI Test Symposium* 194-200 (1993).

26. Chalecka-Franaszek, E. et al. 5-Hydroxytryptamine2A receptor stimulation induces activator protein-1 and cyclic AMP-responsive element binding with cyclic AMP-responsive element-binding protein and Jun D as common components in cerebellar neurons. *Neuroscience*. **88:** 885-898 (1999).

27. Dolmetsch, R. E. *et al.* Signaling to the nucleus by an L-type calcium channel-calmodulin complex through the MAP kinase pathway. *Science*. 294, 333 (2001).

28. D. D. Ginty *et al.,* Regulation of CREB phosphorylation in the suprachiasmatic nucleus by light and a circadian clock. *Science* **260,** 238 (1993).

29. H. Bito, K. Deisseroth, R. W. Tsien, CREB phosphorylation and dephosphorylation: a Ca(2+)- and stimulus duration-dependent switch for hippocampal gene expression. *Cell* **87**, 1203 (1996).

30. Eissing, T. *et al.* Sensitivity analysis of programmed cell death and implications for crosstalk phenomena during Tumor Necrosis Factor stimulation. *Proc. IEEE International Conference on Control Applications* 1746-1752 (2006).

31. Piskulic, D., Olver, J. S., Norman T.R., & Maruff, P. Behavioural studies of spatial working memory dysfunction in schizophrenia: a quantitative literature review. *Psychiatry Res*. **150:** 111-121 (2007).

32. Boehme, K. A., Kulikov, R., & Blattner, C. p53 stabilization in response to DNA damage requires Akt/PKB and DNA-PK. *Proc Natl Acad Sci U S A.* **105:** 7785-7790 (2008).

33. Bachelder, R. E. et al. p53 inhibits alpha 6 beta 4 integrin survival signaling by promoting the caspase 3-dependent cleavage of AKT/PKB. *J Cell Biol.* **147:** 1063-1072 (1999).

34. Sabbatini, P., & McCormick, F. Phosphoinositide 3-OH kinase (PI3K) and PKB/Akt delay the onset of p53-mediated, transcriptionally dependent apoptosis. *J Biol Chem.* **274:** 24263-24269 (1999).

35. Li, H. H., Cai, X., Shouse, G. P., Piluso, L. G., & Liu, X. A specific PP2A regulatory subunit, B56gamma, mediates DNA damage-induced dephosphorylation of p53 at Thr55. *EMBO J.* **26:** 402-411 (2007).

36. Moule, M. G., Collins, C. H., McCormick, F., & Fried, M. Role for PP2A in ARF signaling to p53. *Proc Natl Acad Sci U S A.* **101:** 14063-14066 (2004).

37. Chen, L., Marechal, V., Moreau, J., Levine, A. J., & Chen, J. Proteolytic cleavage of the mdm2 oncoprotein during apoptosis. *J. Biol. Chem.* **272:** 22966-22973 (1997).

38. Herrera-Velit, P. & Reiner, N. E. Bacterial lipopolysaccharide induces the association and coordinate activation of p53/56lyn and phosphatidylinositol 3-kinase in human monocytes. *J Immunol.* **156:** 1157-1165 (1996).

39. Goldman-Rakic, P.S., Lidow, M. S., & Gallager, D. W. Overlap of dopaminergic, adrenergic, and serotoninergic receptors and complementarity of their subtypes in primate prefrontal cortex. *J Neurosci.* **10:** 2125-2138 (1990).

40. Mahgoub, M. A., Sara, Y., Kavalali, E. T., & Monteggia, L. M. Reciprocal interaction of serotonin and neuronal activity in regulation of cAMP-responsive element-dependent gene expression. *J Pharmacol Exp Ther.* **317:** 88-96 (2006).

41. Alagarsamy, S., Phillips, M., Pappas, T., & Johnson, K. M. Dopamine neurotoxicity in cortical neurons. *Drug Alcohol Depend.* **48:** 105-111 (1997).

42. Fatatis, A., & Russell, J. T. Spontaneous changes in intracellular calcium concentration in type I astrocytes from rat cerebral cortex in primary culture. *Glia.***5:** 95-104 (1992).

43. Yu, R., Xu, X. H., & Sheng, M. P. Differential effects of allopregnanolone and GABA on kainate-induced lactate dehydrogenase release in cultured rat cerebral cortical cells. *Acta Pharmacol Sin.* **23:** 680-684 (2002).

44. Nicolas, F., Oillet, J., Koziel, V., & Daval, J. L. Characterization of adenosine receptors in a model of cultured neurons from rat forebrain. *Neurochem Res.* **19:** 507-515 (1994).

45. **Acknowledgement.** We would like to thank Mr. H. Asadi (Northeastern University, Boston) for helping us with the analysis of digital circuits. We also thank Dr. A. Ma'ayan and Dr. R. Iyengar (Mount Sinai School of Medicine, New York) for useful comments regarding the use of their SAVI software tool.

Fig. 1. A toy molecular network. (A) The input molecules of the seven node toy model are *A* and *B*, the intermediate molecules are *C*, *D*, *E*, *F*, and finally *G* is the output molecule. The activatory and inhibitory signals are shown by lines ended to → and ⁄, respectively. (B) Logic equations of the molecular network of Fig. 1A, used to generate the equivalent digital electronic circuit in Fig. 1B. The symbols ×, + and ' in these equations stand for the binary logic operations AND, OR and NOT, respectively. (C) The

digital electronic circuit derived for the molecular network of Fig. 1A. The function of each logic gate (circuit component) is specified in the square box. Names of some molecules in the circuit diagram may appear few times, for the convenience of the reader, to easily recognize the inputs and outputs of the logic gates. A small black dot is used to show where a wire is branched out from another wire.

Fig. 2. The caspase3-FKHR network. (A) The caspase3-FKHR network is based on (5, 6) and has a total of 22 nodes. The input molecules are EGF, insulin, and TNF, and the output molecules are caspase3 and FKHR. The node ComplexI includes TNFR and TRADD-RIP-TRAF2 (5), whereas the node ComplexII stands for TRADD-RIP-TRAF2 and FADD (5). (B) The digital electronic caspase3-FKHR circuit, derived based on the caspase3-FKHR molecular network..

Fig. 3. The p53 network. (A) This network has a total of 49 molecules. The input molecules are insulin and PDGF, and the output molecule is p53. All the 94 intermolecular interactions of this network are listed in the Supplementary Materials, along with literature citations. (B) The vulnerability bar chart of the p53 circuit. The vulnerabilities of PIP2, AKT, caspase3, and PP2A are greater than 0.5, whereas those of caspase8, phosphoinositide 3-kinase (PI3K), Abelson leukemia tyrosine kinase (Abl), phosphatidylinositol 3,4,5 triphosphate (PIP3), the lipid phosphatase PTEN, and protein kinase C (PKC) are between 0.1 and 0.5. The vulnerabilities of the rest of the molecules are less than 0.1. (C) The histogram of the vulnerability values of the p53 circuit. The

number at the top of each bar represents the total number of molecules whose vulnerabilities fall within the range specified by the location of that bar.

Fig. 4. The CREB network. (A) This network has a total of 64 molecules. The input molecules are glutamate, dopamine, GABA, serotonin, ACh, adenosine, and enkephalin, and the output molecule is CREB. .All the 152 intermolecular interactions of this network are listed in the Supplementary Materials, along with literature citations. (B) The vulnerability bar chart of the CREB circuit. The vulnerabilities of calmodulin, Ca^{2+}, cAMP, $G\alpha_i$, AC2, AC1, AC5, PKA, P/Q-type calcium channels, and PP2A are greater than or equal to 0.5, whereas those of $G\beta\gamma$, calcium/calmodulin dependent protein kinase II (CaMKII), protein phosphatase 2B (PP2B), calcium/calmodulin dependent protein kinase type IV (CaMKIV), calmodulin-dependent protein kinase kinase (CaMKK), cAMP response element modulator (CREM), N-type calcium channels (abbreviated N-type CaCh in circuit), N-methyl-D-aspartate type glutamate receptor (NMDAR), PI3K, PIP3, the kinase PDK1, and the kinase RSK are between 0.1 and 0.5. The vulnerabilities of the rest of the molecules are less than 0.1. (C) The histogram of the vulnerability values of the CREB circuit. The number at the top of each bar represents the total number of molecules whose vulnerabilities fall within the range specified by the location of that bar.

Fig. 5. Experimental verification of the fault diagnosis findings. (A) Western blot analysis on the protein extracts from primary neuronal culture after 2.5 and 12 hours treatment with either vehicle or 1 μM concentration of the selective P/Q-type calcium

channel blocker, ω-Agatoxin IVA. Each blot shown in this figure is a representative blot of three independent experiments. (B) 48 hours following adenoviral transduction using three unique shRNA constructs targeting P/Q-type calcium channels. Lane 1 shows the protein size by a protein marker (Magic Marker from Invitrogen). Lanes 2 and 6 are loaded with protein extracts from two control plates (mock) and lanes 3, 4 and 5 are treated with V1, V2, and V3 adenoviral vectors, respectively. Top blot shows a decrease in P/Q-type calcium channel abundance with V2 vector (lane 4) and a smaller decrease with the V1 vector (lane 3). Middle blots show the total protein and Ser^{133} phosphorylation of CREB in the same set of samples. The same membrane of the top blot was stripped and re-probed with anti-CREB antibody. Bottom blot shows total actin protein of the same membrane, as the loading control. (C) After 2 hours treatment with 0.1 or 0.2 μg/ml of the $G\alpha_i$ antagonist, pertussis toxin, and 5 or 10 μM of $G\alpha_i$ agonist, MAS-7. Blots were first probed with antibody against phospho-CREB (Ser^{133}) (top) then stripped and re-probed with antibody against CREB (middle) and the antibody against actin (bottom), as the loading control for confirming equal loading. (D) The activity of CREB following treatment with different neurotransmitter ligands, including serotonin (STN), glutamate (GLT), dopamine (DPM), GABA, and adenosine (ADN). Top blot shows phosphorylation of CREB at Ser^{133}, 15 minutes after treatment with vehicle,10 μM forskolin (FSK), serotonin, glutamate, dopamine, GABA, and adenosine, respectively. Middle blot shows total CREB protein on the same blot. Bottom blot shows actin as loading control. (E) The effect of treatment with serotonin on the CREB activity when PKA is activated with forskolin or inhibited with H-89. Cells were treated with vehicle, 10 μM forskolin or H-89 for 30 minutes followed by 15 minutes treatment with 10 μM

serotonin. (F) Immunofluorescent analysis of primary cortical culture following treatment with vehicle, forskolin, serotonin, or serotonin and forskolin. Red represents the phosphorylated CREB (Ser^{133}) as a measure of CREB activity. Green represents the Map-2 staining as a specific neuronal marker and blue represent DRAQ-5 nuclear staining of all the cells in the primary culture (both neuronal and glial cells). Images were captured with the same confocal parameters for the four different treatment conditions.

Table 1. Truth table of the caspase3-FKHR digital circuit (Fig. 2B). It shows the binary logic values of the outputs, FKHR and caspase3, when different inputs are applied to the circuit. The first three columns include all possible input scenarios, whereas the last three columns are computed according to circuit logic equations (Supplementary Table 1) and the basic properties of binary operations as described in the text.

Table 2. The vulnerability values of the caspase3-FKHR circuit and the caspase3 circuit in which the output node FKHR and its preceding BUFFER are removed. The vulnerabilities are calculated using the EPP algorithm (8,9), and are sorted from high to low. In both circuits, AKT has the highest vulnerability value.

Table 3. The vulnerability values of the p53 circuit, calculated using the EPP algorithm and sorted from high to low.

Table 4. The vulnerability values of the CREB circuit, calculated using the EPP algorithm and sorted from high to low.

A

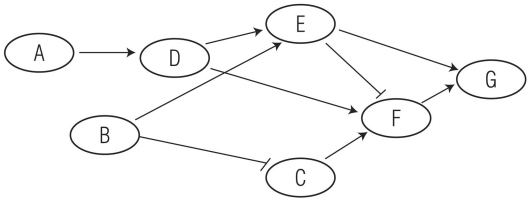

B

$C = B'$
$D = A$
$E = B + D$
$F = E' \times (C+D)$
$G = E + F$

x : AND binary logic operation
+ : OR binary logic operation
' : NOT binary logic operation

C

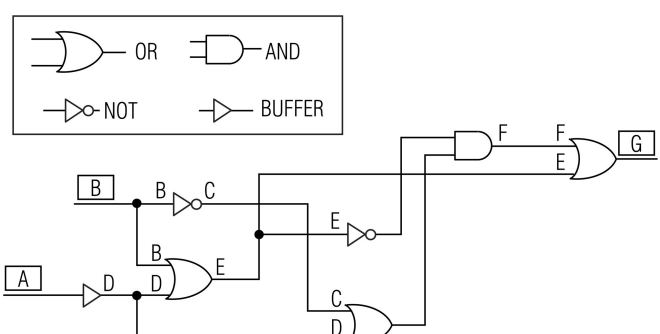

Abdi et al., Fig. 1

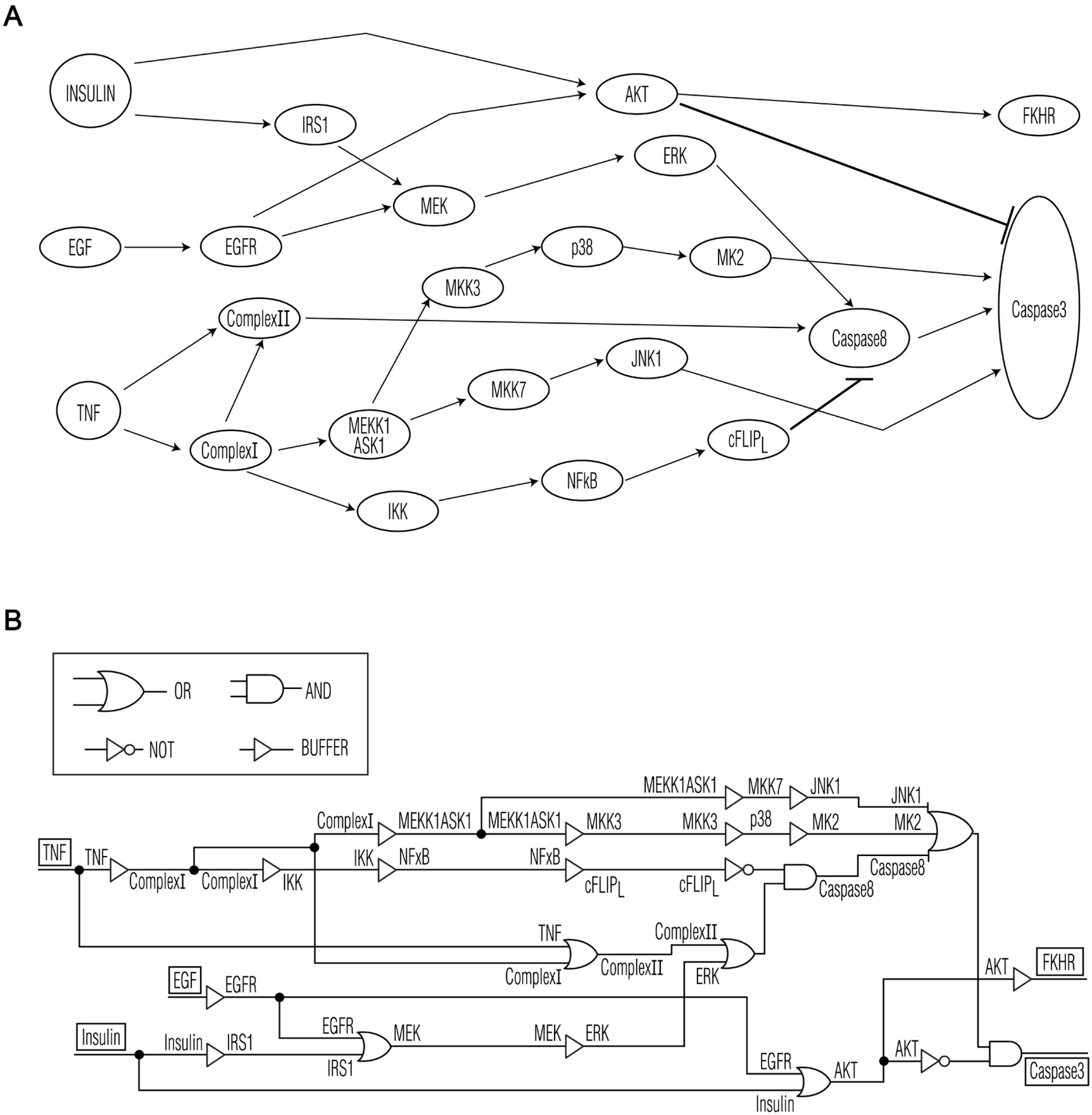

Abdi et al., Fig. 2

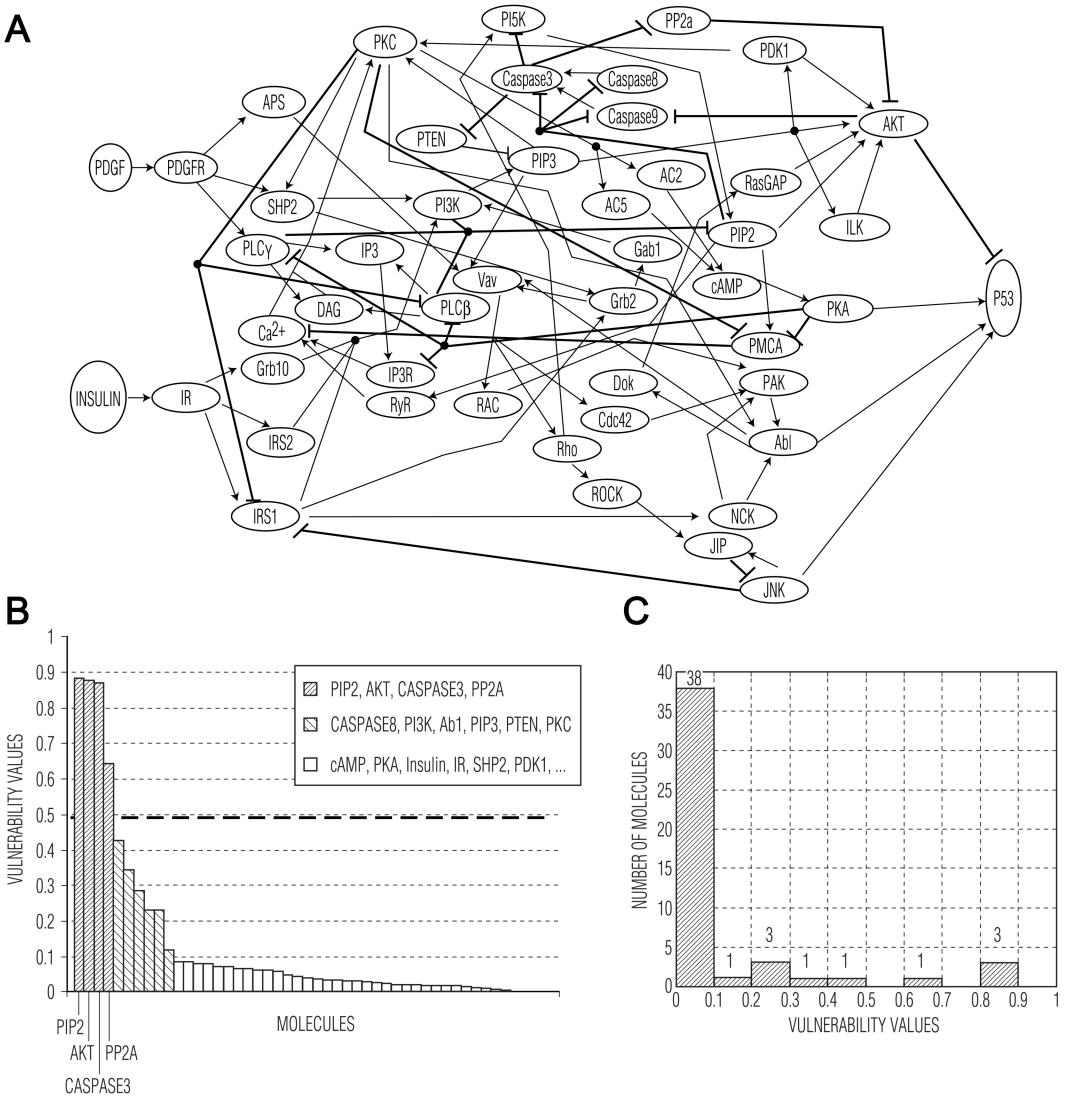

Abdi et al., Fig. 3

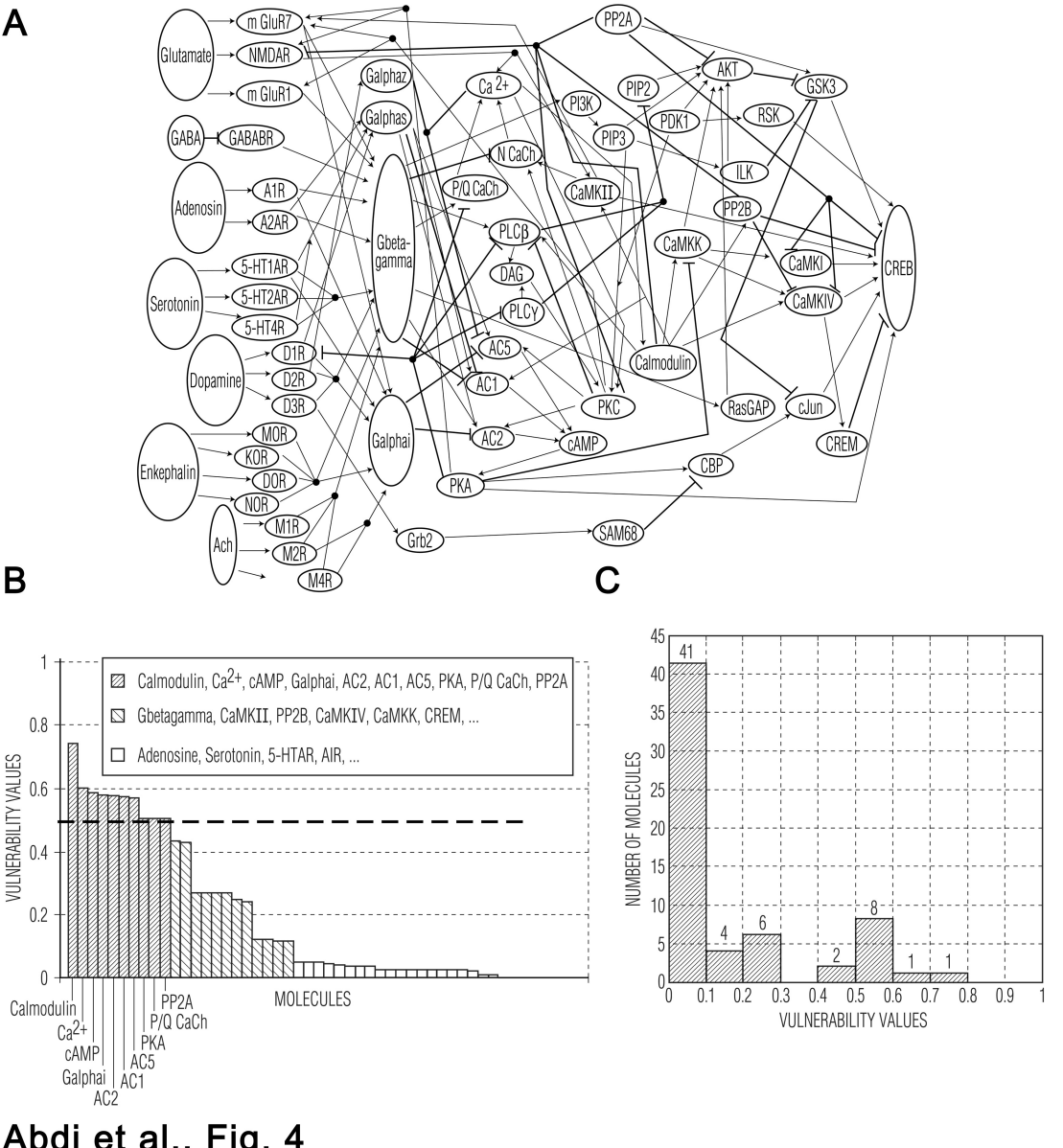

Abdi et al., Fig. 4

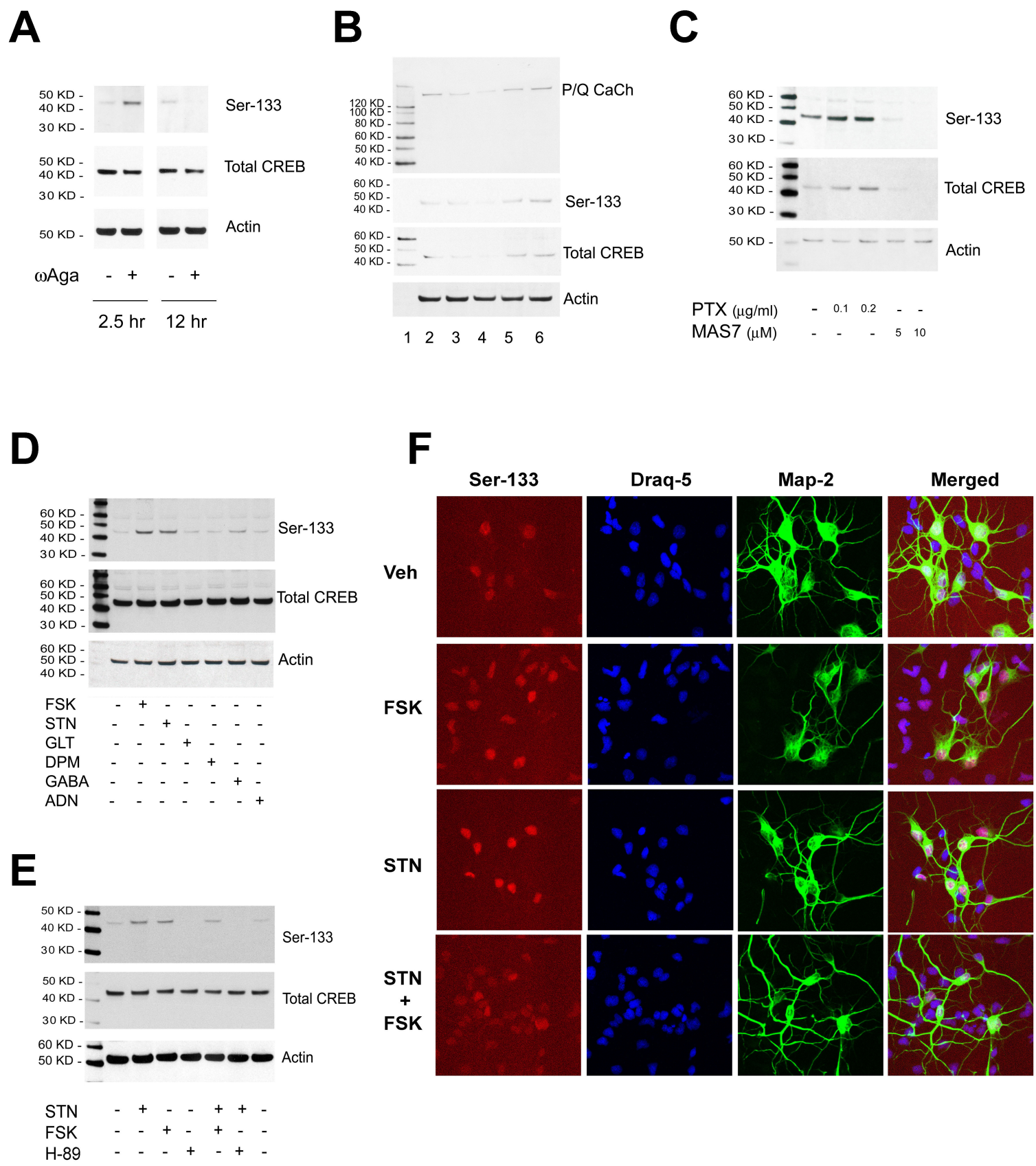

Abdi et al., Fig. 5

EGF	INSULIN	TNF	FKHR	CASPASE3	CASPASE3 (AKT IS STUCK AT 1)
0	0	0	0	0	0
0	0	1	0	1	0
0	1	0	1	0	0
0	1	1	1	0	0
1	0	0	1	0	0
1	0	1	1	0	0
1	1	0	1	0	0
1	1	1	1	0	0

Abdi et al., Table 1

NODE	VUL. (WITH FKHR)	VUL. (WITHOUT FKHR)
CASPASE3	1	1
FKHR	1	–
AKT	1	0.874
EGF	0.5	0.249
EGFR	0.5	0.249
Insulin	0.49	0.245
MEKK1ASK1	0.249	0.249
TNF	0.249	0.249
ComplexI	0.125	0.125
ComplexII	0.125	0.125
ERK	0.125	0.125
IRS1	0.125	0.125
JNK1	0.125	0.125
MEK	0.125	0.125
MK2	0.125	0.125
MKK3	0.125	0.125
MKK7	0.125	0.125
CASPASE8	0.125	0.125
p38	0.125	0.125
IKK	0	0
NFKB	0	0
cFLIPL	0	0

Abdi et al., Table 2

NODE	VUL.	NODE	VUL.	NODE	VUL.
p53	1	Dok	0.067	ROCK	0.022
PIP2	0.88	RasGAP	0.067	IRS1	0.021
AKT	0.88	AC2	0.064	Gab1	0.019
CASPASE3	0.87	ILK	0.062	RyR	0.018
PP2A	0.64	Vav	0.061	PDGF	0.017
CASPASE8	0.43	PLCβ	0.05	PDGFR	0.017
P13K	0.35	Ca^{2+}	0.046	IP3	0.015
Abl	0.29	AC5	0.042	DAG	0.013
PIP3	0.23	Rho	0.038	PMCA	0.011
PTEN	0.23	Grb10	0.036	CASPASE9	0.007
PKC	0.12	IRS2	0.036	Grb2	0.0052
cAMP	0.086	PLCy	0.033	Cdc42	0.0015
PKA	0.086	PIP5K	0.032	Rac	0.0015
Insulin	0.082	IP3R	0.029	APS	0.00025
IR	0.082	PAK	0.026	NCK	0.00012
SHP2	0.073	JNK	0.023		
PDK1	0.071	JIP	0.023		

Abdi et al., Table 3

NODE	VUL.	NODE	VUL.	NODE	VUL.
CREB	1	RSK	0.12	A2AR	0
Calmodulin	0.74	Adenosine	0.05	CaMKI	0
CA^{2+}	0.6	Serotonin	0.05	CBP	0
cAMP	0.59	5-HT1AR	0.05	cJun	0
Galphai	0.58	A1R	0.045	DAG	0
AC2	0.58	Dopamine	0.04	5-HT2AR	0
AC1	0.57	Ach	0.035	5-HT4R	0
AC5	0.57	Enkephalin	0.035	GABABR	0
PKA	0.5	mGluR7	0.035	Galphas	0
P/Q type CaCh	0.5	D1R	0.025	Grb2	0
PP2A	0.5	D2R	0.025	GSK3	0
Gbetagamma	0.43	D3R	0.025	ILK	0
CaMKII	0.43	D0R	0.025	M1R	0
PP2B	0.27	K0R	0.025	PIP2	0
CaMKIV	0.27	M2R	0.025	AKT	0
CaMKK	0.27	M4R	0.025	PKC	0
CREM	0.27	M0R	0.025	PLCβ	0
N-type CaCh	0.25	N0R	0.025	PLCγ	0
NMDAR	0.24	Galphaz	0.02	RasGAP	0
P13K	0.12	Glutamate	0.01	SAM68	0
PIP3	0.12	mGluR1	0.01		
PDK1	0.12	GABA	0		

Abdi et al., Table 4

Supplementary Materials

Vulnerability assessment algorithm

Here we summarize our molecular vulnerability assessment algorithm, through which the vulnerability of a cellular signaling network to the dysfunction of its components can be calculated. The details of each step are explained in the Method Section.

1- Specify the inputs nodes (such as ligands, receptors, secondary messengers, etc.) and the output nodes (such as different transcription factors relevant to the input signal), as well as the intermediate molecules that allow the input signals to propagate from the inputs to the outputs. Then specify the type of the interactions among the molecules (stimulatory or inhibitory), using the existing literature.

2- Use Rule #1 and Rule #2, to derive a binary logic equation for every intermediate molecule and the output molecules, using the interactions specified in Step 1.

3- Construct the digital circuit of the network from the binary logic equations of Step 2, using the AND, OR, NOT and BUFFER digital circuit elements.

4- Identify the feedback paths of the digital circuit of Step 3, using the depth-first search (DFS) algorithm. If there is no feedback path, proceed directly to the next step.

5- Finally, apply the EPP algorithm to the circuit obtained in the previous step, to calculate the vulnerability levels of all the input and intermediate nodes (the vulnerability of the output node is always 1, since if the output node is dysfunctional, the network will not operate efficiently anyway).

Deriving the logic equations

The logic equation of each molecule is a symbolic Boolean expression that shows how the activity of the molecule is regulated by its inputs. Using Rule #1 and Rule #2, a binary logic equation for each intermediate molecule and the output molecule were obtained, in terms of the input stimulators and inhibitors. These two rules are devised based on the known physiological mechanisms that different regulators employ to control the activity of signaling molecules. Rule #1 applies the Boolean OR of activating inputs to a signaling network. Rule #2 applies the Boolean AND of inverted inhibitory inputs to the network. In the derived equations for the networks, ', + and × stand for the binary logic operations NOT, OR and AND, respectively.

Constructing the digital circuits

To obtain the digital circuit schematic of a set of logic equations for a particular network, the ', + and × operations were represented in the circuit by NOT, OR and AND circuit components, respectively. Equations of the form $X = Y$, where X and Y are two different molecules and X is activated by Y, were implemented using the BUFFER circuit component.

Molecule	Logic equation
AKT	AKT=EGFR+Insulin
Caspase3	Caspase3=AKT'×(Caspase8+JNK1+MK2)
Caspase8	Caspase8=$cFLIP_L$'×(ComplexII+ERK)
$cFLIP_L$	$cFLIP_L$=NFκB
ComplexI	ComplexI=TNF
ComplexII	ComplexII=TNF+ComplexI
EGFR	EGFR=EGF
ERK	ERK=MEK
FKHR	FKHR=AKT
IKK	IKK=ComplexI
IRS1	IRS1=Insulin
JNK1	JNK1=MKK7
MEK	MEK=EGFR+IRS1
MEKK1ASK1	MEKK1ASK1=ComplexI
MK2	MK2=p38
MKK3	MKK3=MEKK1ASK1
MKK7	MKK7=MEKK1ASK1
NFκB	NFκB=IKK
P38	p38=MKK3

Supplementary Table 1. Logic equations of the caspase3-FKHR network. Each logic equation specifies the input signals to a molecule using the logic operations ', + and ×, which represent NOT, OR and AND, respectively. These equations are used to generate the digital electronic caspase3-FKHR circuit (Fig. 2B).

Abl to Dok[167], Abl to p53[43,83,104], Abl to Vav[8], AC2 to cAMP[38], AC5 to cAMP[60], AKT to CASPASE9[17], AKT to p53[50,90,119,121,125,166], APS to Vav[164], Ca^{2+} to AC5[58], Ca^{2+} to PKC[141], cAMP to PKA[87], CASPASE3 to PIP5K[94], CASPASE3 to PP2A[72,117], CASPASE3 to PTEN[26,147], CASPASE8 to CASPASE3[18,38,84,130], CASPASE9 to CASPASE3[78,103,128], Cdc42 to PAK[5], DAG to PKC[141], Dok to RasGAP[55], Gab1 to PI3K[54], Grb10 to PI3K[31], Grb2 to Gab1[54], Grb2 to Vav[171], ILK to AKT[30], Insulin to IR[149], IP3 to IP3R[114], IP3R to Ca^{2+} [139], IR to Grb10[31], IR to IRS1[137], IR to IRS2[4], IRS1 to Grb2[126], IRS1 to NCK[74], IRS1 to PI3K[47], IRS2 to PI3K[165], JIP to JNK[34], JNK to IRS1[99], JNK to JIP[27], JNK to p53[1], NCK to Abl[127], NCK to PAK[85], PAK to Abl[113], PDGF to PDGFR[68], PDGFR to APS[172], PDGFR to PLCγ[93], PDGFR to SHP2[134], PDK1 to AKT[2], PDK1 to PKC[35], PI3K to PIP3[159], PIP2 to AKT[133], PIP2 to CASPASE3[94], PIP2 to CASPASE8[94,112], PIP2 to CASPASE9[94], PIP2 to PMCA[52], PIP2 to RyR[19], PIP3 to AKT[133], PIP3 to ILK[30], PIP3 to PDK1[2], PIP3 to PKC[124], PIP3 to Vav[49], PIP3K to PIP2[159], PIP5K to PIP2[14], PKA to IP3R[139], PKA to p53[1], PKA to PLCβ[82], PKA to PLCγ[69], PKA to PMCA[177], PKC to Abl[136], PKC to AC2[174], PKC to AC5[67], PKC to IRS1[96], PKC to PLCβ[81], PKC to PMCA[148], PKC to SHP2[99], PLCβ to DAG[15], PLCβ to IP3[15], PLCβ to PIP2[116], PLCγ to DAG[131], PLCγ to IP3[131], PLCγ to PIP2[93], PMCA to Ca^{2+} [105], PP2A to AKT[11,98,151], PTEN to PIP3[77,110], Rac to PAK[88], RasGAP to AKT[175], Rho to PIP5K[111], Rho to ROCK[101], Rock to JIP[27], RyR to Ca^{2+} [59], SHP2 to Gab1[64], SHP2 to Grb2[144], SHP2 to PI3K[156], Vav to Cdc42[109], Vav to Rac[23], Vav to Rho[120]

Supplementary Fig. 1. Intermolecular interactions of the p53 network.
This network (Fig. 3A) includes the above 94 interactions, listed alphabetically, according to the name of *"source"* molecules. At least one representative reference from the national library of medicine (Pub Med) is listed for each individual interaction. These references are listed at the end of the Supplementary Materials.

Molecule	Logic equation
Abl	Abl=NCK+PKC+PAK
AC2	AC2=PKC
AC5	AC5=(Ca^{2+})'×PKC
APS	APS=PDGFR
Ca^{2+}	Ca^{2+}=PMCA'×(IP3R+RyR)
cAMP	cAMP=AC2+AC5
CASPASE3	CASPASE3=PIP2'×(CASPASE8+CASPASE9)
CASPASE8	CASPASE8=PIP2'
CASPASE9	CASPASE9=PIP2'×AKT'
Cdc42	Cdc42=Vav
DAG	DAG=PLCβ+PLCγ
Dok	Dok=Abl
Gab1	Gab1=SHP2'×Grb2
Grb2	Grb2=IRS1+SHP2
Grb10	Grb10=IR

ILK	ILK=PIP3
IP3	IP3=PLCβ+PLCγ
IP3R	IP3R=PKA'×IP3
IR	IR=Insulin
IRS1	IRS1=JNK'×PKC'×IR
IRS2	IRS2=IR
JIP	JIP=ROCK+JNK
JNK	JNK=JIP'
NCK	NCK=IRS1
p53	p53=AKT'×(Abl+PKA+JNK)
PAK	PAK=Cdc42+NCK+Rac
PDK1	PDK1=PIP3
PDGFR	PDGFR=PDGF
PI3K	PI3K=Gab1+Grb10+IRS1+IRS2+SHP2
PIP2	PIP2=PI3K'×PLCβ'×PLCγ'×PIP5K
PIP3	PIP3=PTEN'×PI3K
PIP5K	PIP5K=CASPASE3'×Rho
PKA	PKA=cAMP
AKT	AKT=PP2A'×(ILK+PDK1+PIP2+PIP3+RasGAP)
PKC	PKC=PDK1+PIP3+DAG+Ca^{2+}
PLCβ	PLCβ=PKA'×PKC'
PLCγ	PLCγ=PKA'×PDGFR
PMCA	PMCA=PKA'×PKC'×PIP2
PP2A	PP2A=CASPASE3'
PTEN	PTEN=CASPASE3'
Rac	Rac=Vav
RasGAP	RasGAP=Dok
Rho	Rho=Vav
ROCK	ROCK=Rho
RyR	RyR=PIP2
SHP2	SHP2=PDGFR+PKC
Vav	Vav=Abl+APS+Grb2+PIP3

Supplementary Table 2. **Logic equations of the p53 network.** Each logic equation specifies the input signals to a molecule using the logic operations ', + and ×, which represent NOT, OR and AND, respectively. These equations are used to generate the digital p53 circuit (Supplementary Fig. 2).

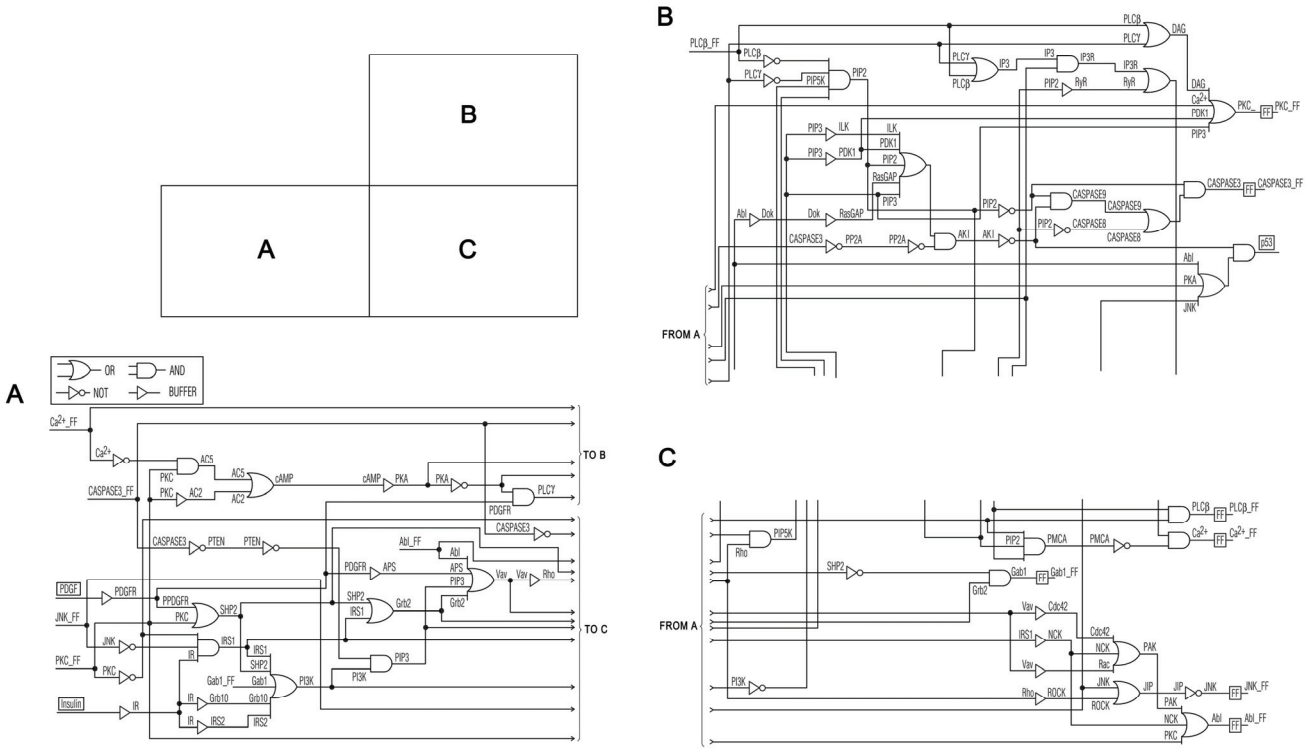

Supplementary Circuit p53

Supplementary Fig. 2. The digital electronic p53 circuit. There are seven feedback paths in this circuit, initiated from the following nodes: Ca^{2+}, JNK, caspase3, Gab1, PLCβ, Abl, and PKC. These feedbacks are identified using the DFS algorithm, and then one flip-flop (FF) is inserted in each path (FF is a one-bit digital logic memory unit). For example, there is an FF at the upper right corner of the circuit, with PKC and PKC_FF as its input and output, respectively. The name PKC_FF appears again at the lower left corner of the circuit, which means that PKC is "fed back" from the right side of the circuit to the left side. The feedback wire itself is not shown, to make the circuit diagram easier to read.

5-HT1AR to Galphas[28], 5-HT1AR to Galphaz[7], 5-HT1AR to Gbetagamma[28], 5-HT2AR to Gbetagamma[20], 5-HT4R to Galphas[12], 5-HT4R to Gbetagamma[12], A1R to Galphai[22], A1R to Gbetagamma[22], A2AR to Galphas[107], A2AR to Galphas[107], A2AR to Gbetagamma[107], AC1 to cAMP[143], AC2 to cAMP[38], AC5 to cAMP[60], Ach to M1R[10], Ach to M2R[13], Ach to M4R[150], Adenosine to A1R[22], Adenosine to A2AR[79], AKT to GSK3[25], Ca^{2+} to AC5[58], Ca^{2+} to Calmodulin[154], Ca^{2+} to PKC[141], Calmodulin to AC1[161], Calmodulin to CaMKII[95], Calmodulin to CaMKIV[63], Calmodulin to CaMKK[91], Calmodulin to $mGluR_7$[102], Calmodulin to NMDAR[76], Calmodulin to PLCβ[92], Calmodulin to PP2B[70], CaMKI to CREB[122], CaMKII to CREB[122], CaMKII to N-type CaCh[173], CaMKII to PP2A[42], CaMKIV to CREB[37], CaMKIV to CREM[138], CaMKK to AKT[170], CaMKK to CaMKI[91], CaMKK to CaMKIV[36], cAMP to PKA[87], CBP to cJun[6], cJun to CREB[48], CREM to CREB[41], D1R to Galphai[123], D1R to Galphas[123], D1R to Gbetagamma[123], D2R to Galphai[45], D2R to Galphaz[106], D2R to Gbetagamma[169], D3R to Galphai[9], D3R to Gbetagamma[9], D3R to Grb2[108], DAG to PKC[141], Dopamine to D1R[45], Dopamine to D2R[45], Dopamine to D3R[9], DOR to Galphai[3], DOR to Gbetagamma[3], Enkephalin to DOR[3], Enkephalin to KOR[3], Enkephalin to MOR[3], Enkephalin to NOR[3], GABA to GABABR[66], GABABR to Gbetagamma[62], Galphai to AC2[145], Galphai to AC5[145], Galphas to AC1[115], Galphas to AC2[38], Galphas to AC5[33], Galphaz to AC1[73], Galphaz to AC5[73], Gbetagamma to AC1[143], Gbetagamma to AC2[142], Gbetagamma to N-type CaCh[29], Gbetagamma to P/Q-type CaCh[29], Gbetagamma to PI3K[132], Gbetagamma to PLCβ[16], Gbetagamma to RasGAP[163], Glutamate to $mGluR_1$[135], Glutamate to $mGluR_7$[102], Glutamate to NMDAR[50], Grb2 to SAM68[100], GSK3 to cJun[155], GSK3 to CREB[40], ILK to AKT[30], ILK to GSK3[30], KOR to Gbetagamma[3], M1R to Gbetagamma[24], M2R to Galphai[168], M2R to Gbetagamma[168], M4R to Galphai[150], M4R to Gbetagamma[150], $mGluR_1$ to Gbetagamma[89], $mGluR_7$ to Galphai[102], $mGluR_7$ to Gbetagamma[102], MOR to Gbetagamma[3], NMDAR to Ca^{2+} [86], NMDAR to CaMKII[76], NMDAR to PLCγ[46], NOR to Gbetagamma[3], N-type CaCh to Ca^{2+} [157], P/Q-type CaCh to Ca^{2+} [53], PDK1 to AKT[2], PDK1 to PKC[35], PDK1 to RSK[61], PI3K to PIP2[159], PI3K to PIP3[159], PIP2 to AKT[133], PIP3 to AKT[133], PIP3 to ILK[30], PIP3 to PDK1[2], PIP3 to PKC[124], PKA to CaMKK[91], PKA to CBP[21], PKA to CREB[97], PKA to D1R[176], PKA to $mGluR_7$[129], PKA to NMDAR[75], PKA to P/Q-type CaCh[160], PKA to PLCβ[82], PKA to PLCγ[69], PKC to AC2[174], PKC to AC5[67], PKC to GSK3[44], PKC to $mGluR_1$[118], PKC to $mGluR_7$[102], PKC to NMDAR[146], PKC to N-type CaCh[140], PKC to PLCβ[81], PLCβ to DAG[15], PLCβ to PIP2[116], PLCγ to DAG[131], PLCγ to PIP2[93], PP2A to AKT[98], PP2A to CaMKI[32], PP2A to CaMKIV[158], PP2A to CREB[152], PP2A to GSK3[25], PP2A to NMDAR[153], PP2B to CaMKIV[65], PP2B to CREB[57], PP2B to NMDAR[80], RasGAP to AKT[175], RSK to CREB[162], SAM68 to CBP[56], Serotonin to 5-HT1AR[71], Serotonin to 5-HT2AR[20], Serotonin to 5-HT4R[12]

Supplementary Fig. 3. Intermolecular interactions of the CREB network.
This network (Fig. 4A) includes 152 interactions, listed alphabetically according to the name of *"source"* molecules. At least one representative reference from the national library of medicine (Pub Med) is listed for each individual interaction. These references are listed at the end of the Supplementary Materials.

Molecule	Logic equation
A1R	A1R=Adenosine
A2AR	A2AR=Adenosine
AC1	AC1=Gbetagamma'×Galphaz'×(Galphas+Calmodulin)
AC2	AC2=Galphai'×(Gbetagamma+Galphas+PKC)
AC5	AC5=Galphai'×Galphaz'×(Ca^{2+})'×(PKC+Galphas)
PP2B	PP2B=Calmodulin
Ca^{2+}	Ca^{2+}=NMDAR+N-typeCaCh+P/QtypeCaCh
Calmodulin	Calmodulin=Ca^{2+}
CaMKI	CaMKI=PP2A'×CaMKK
CaMKII	CaMKII=Calmodulin+NMDAR
CaMKIV	CaMKIV=PP2A'×PP2B'×(Calmodulin+CaMKK)
CaMKK	CaMKK=PKA'×Calmodulin
cAMP	cAMP=AC1+AC2+AC5
CBP	CBP=SAM68'×PKA
cJun	cJun=GSK3'×CBP
CREB	CREB=PP2A'×PP2B'×CREM'×(GSK3+PKA+cJun+RSK+CaMKII +CaMKIV+CaMKI)
CREM	CREM=CaMKIV
D1R	D1R=PKA'×Dopamine
D2R	D2R=Dopamine
D3R	D3R=Dopamine
DAG	DAG=PLCβ+PLCγ
DOR	DOR=Enkephalin
5-HT1AR	5-HT1AR=Serotonin
5-HT2AR	5-HT2AR=Serotonin
5-HT4R	5-HT4R=Serotonin
GABABR	GABABR=GABA'
Galphai	Galphai=A1R+D1R+D2R+D3R+M4R+M2R+$mGluR_7$+DOR+KOR +MOR+NOR+5-HT1AR
Galphas	Galphas=A2AR+D1R+5-HT1AR+5-HT4R
Galphaz	Galphaz=D2R+5-HT1AR
Gbetagamma	Gbetagamma=A1R+A2AR+M1R+M4R+M2R+D1R+D2R+D3R +GABABR+$mGluR_1$+$mGluR_7$+DOR+KOR+MOR+NOR +5-HT1AR+5-HT2AR+5-HT4R
Grb2	Grb2=D3R
GSK3	GSK3=ILK'×AKT'×PKC'×PP2A
ILK	ILK=PIP3
KOR	KOR=Enkephalin
M1R	M1R=Ach
M2R	M2R=Ach
M4R	M4R=Ach
$mGluR_1$	$mGluR_1$=PKC+Glutamate

$mGluR_7$	$mGluR_7$=Calmodulin'×(PKC+PKA+Glutamate)
MOR	MOR=Enkephalin
NMDAR	NMDAR=PKC'×PP2A'×Calmodulin'×PP2B'×(PKA+Glutamate)
NOR	NOR=Enkephalin
N-type CaCh	N-typeCaCh=Gbetagamma'×(PKC+CaMKII)
PDK1	PDK1=PIP3
PI3K	PI3K=Gbetagamma
PIP2	PIP2=PI3K'×PLCβ'×PLCγ'
PIP3	PIP3=PI3K
PKA	PKA=cAMP
AKT	AKT=PP2A'×(RasGAP+ILK+PIP3+PDK1+PIP2+CaMKK)
PKC	PKC=PDK1+PIP3+DAG+Ca^{2+}
PLCβ	PLCβ=PKA'×PKC'×(Gbetagamma+Calmodulin)
PLCγ	PLCγ=PKA'×NMDAR
PP2A	PP2A=CaMKII'
P/Q type CaCh	P/QtypeCaCh=PKA'×Gbetagamma
RasGAP	RasGAP=Gbetagamma
RSK	RSK=PDK1
SAM68	SAM68=Grb2

Supplementary Table 3. Logic equations of the CREB network. Each logic equation specifies the input signals to a molecule using the logic operations ', + and ×, which represent NOT, OR and AND, respectively. These equations are used to generate the digital electronic CREB circuit (Supplementary Fig. 4).

Supplementary Fig. 4. The digital electronic CREB circuit (see next page). There are five feedback paths in this circuit, initiated from the following nodes: PLCγ, PP2A, calmodulin, PKA and PKC. These feedbacks are identified using the DFS algorithm, and then one flip-flop (FF) is inserted in each path. For example, there is an FF at the upper right corner of the circuit, with PKA and PKA_FF as its input and output, respectively. The name PKA_FF is appeared again at the upper left corner of the circuit, which means that PKA is "fed back" from the right side of the circuit to the left side. The feedback wire itself is not shown, to make the circuit diagram easier to read.

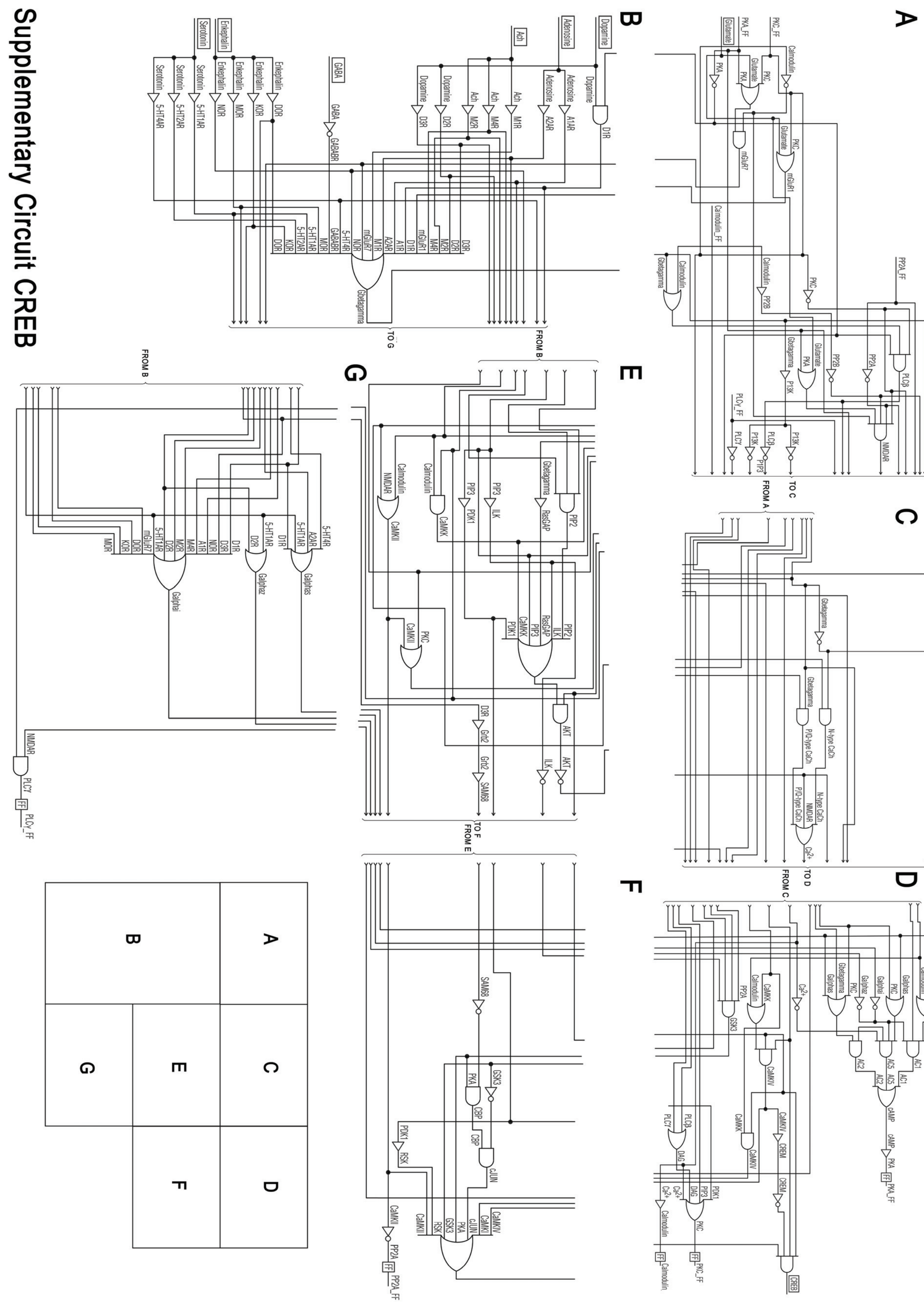
Supplementary Circuit CREB
A
B
C
D
E
F
G

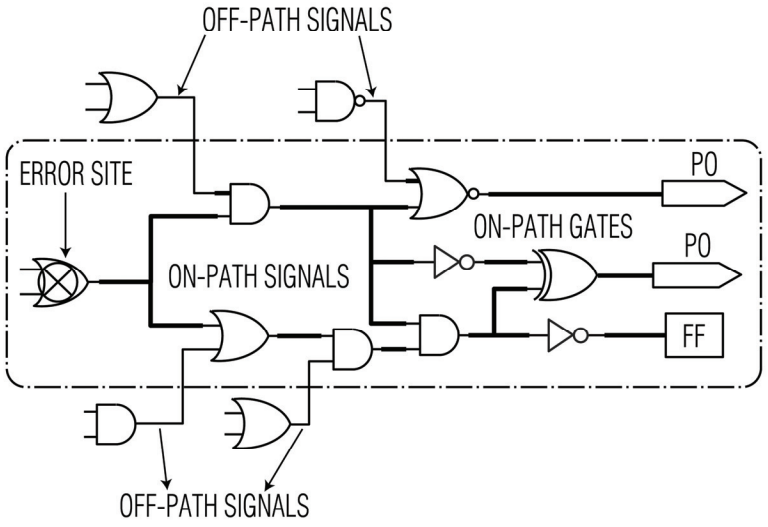

Supplementary Fig. 5

Supplementary Fig. 5. A typical path between an erroneous node to primary outputs and flip-flops.

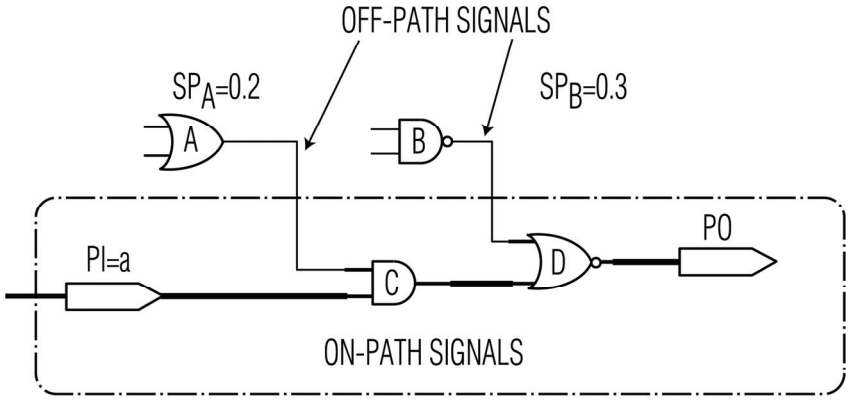

Supplementary Fig. 6

Supplementary Fig. 6. A simple path between an erroneous input to a primary output.

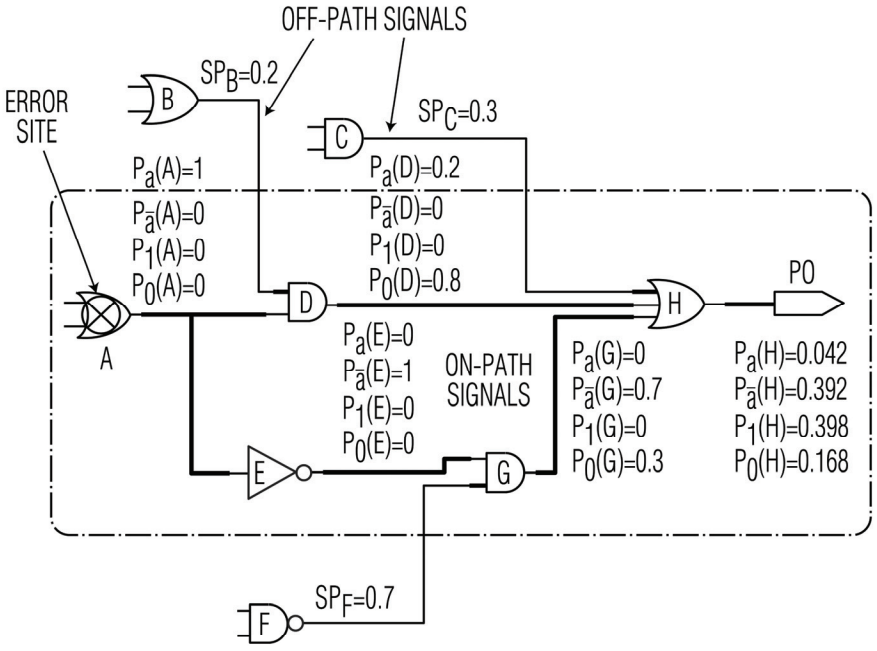

Supplementary Fig. 7

Supplementary Fig. 7. Applying error propagation rules for a reconverging path.

AND	$P_1(out) = \prod_{i=1}^{n} P_1(X_i)$ $P_a(out) = \prod_{i=1}^{n} [P_1(X_i) + P_a(X_i)] - P_1(out)$ $P_{\bar{a}}(out) = \prod_{i=1}^{n} [P_1(X_i) + P_{\bar{a}}(X_i)] - P_1(out)$ $P_0(out) = 1 - [P_1(out) + P_a(out) + P_{\bar{a}}(out)]$
OR	$P_0(out) = \prod_{i=1}^{n} P_0(X_i)$ $P_a(out) = \prod_{i=1}^{n} [P_0(X_i) + P_a(X_i)] - P_0(out)$ $P_{\bar{a}}(out) = \prod_{i=1}^{n} [P_0(X_i) + P_{\bar{a}}(X_i)] - P_0(out)$ $P_1(out) = 1 - [P_0(out) + P_a(out) + P_{\bar{a}}(out)]$
NOT	$P_0(out) = P_1(in)$, $P_1(out) = P_0(in)$ $P_a(out) = P_{\bar{a}}(in)$, $P_{\bar{a}}(out) = P_a(in)$

Supplementary Table 4. Computing probability at the output of a gate in terms of its inputs.

Supplementary References

1. Adler, V. *et al.* Conformation-dependent phosphorylation of p53. Proc. Natl. Acad. Sci. U. S. A. 94, 1686 (1997).
2. Alessi, D. R. *et al.* Characterization of a 3-phosphoinositide-dependent protein kinase which phosphorylates and activates protein kinase Balpha. Curr. Biol. 7, 261 (1997).
3. Alexander, S. P. *et al.* Guide to receptors and channels, 1st edition. Br. J. Pharmacol. 141, S1 (2004).
4. Araki, E. *et al.* Alternative pathway of insulin signalling in mice with targeted disruption of the IRS-1 gene. Nature. 372, 186 (1994).
5. Bagrodia, S. *et al.* Cdc42 and PAK-mediated signaling leads to Jun kinase and p38 mitogen-activated protein kinase activation. J. Biol. Chem. 270, 27995 (1996).
6. Bannister, A. J. *et al.* Stimulation of c-Jun activity by CBP: c-Jun residues Ser63/73 are required for CBP induced stimulation in vivo and CBP binding in vitro. Oncogene. 11, 2509 (1996).
7. Barr, A. J. & Manning, D. R. Agonist-independent activation of Gz by the 5-hydroxytryptamine1A receptor co-expressed in Spodoptera frugiperda cells. Distinguishing inverse agonists from neutral antagonists. J. Biol. Chem. 272, 32979 (1998).
8. Bassermann, F. *et al.* Association of Bcr-Abl with the proto-oncogene Vav is implicated in activation of the Rac-1 pathway. J. Biol. Chem. 277, 12437 (2002).
9. Beom, S. *et al.* Comparative studies of molecular mechanisms of dopamine D2 and D3 receptors for the activation of extracellular signal-regulated kinase. J. Biol. Chem. 279, 28304 (2004).
10. Berstein, G. *et al.* Reconstitution of agonist-stimulated phosphatidylinositol 4,5-bisphosphate hydrolysis using purified m1 muscarinic receptor, Gq/11, and phospholipase C-beta 1. J. Biol. Chem. 267, 8081 (1992).
11. Bjornsti, M.-A. & Houghton, P. J. The tor pathway: A target for cancer therapy. Nature Rev. Cancer. 4, 335 (2004).
12. Bockaert, J. *et al.* Pharmacological characterization of 5-hydroxytryptamine4(5-HT4) receptors positively coupled to adenylate cyclase in adult guinea pig hippocampal membranes: effect of substituted benzamide derivatives. Mol. Pharmacol. 37, 408 (1990).
13. Bonner, T. I. *et al.* Identification of a family of muscarinic acetylcholine receptor genes. Science. 237, 527 (1987).
14. Boronenkov, I. V. & Anderson, R. A. The sequence of phosphatidylinositol-4-phosphate 5-kinase defines a novel family of lipid kinases. J. Biol. Chem. 270, 2881 (1995).

15. Burgess, G. M. *et al.* The second messenger linking receptor activation to internal Ca release in liver. Nature. 309, 63 (1984).

16. Camps, M. *et al.* Isozyme-selective stimulation of phospholipase C-beta 2 by G protein beta gamma-subunits. Nature. 360, 684 (1993).

17. Cardone, M. H. *et al.* Regulation of cell death protease caspase-9 by phosphorylation. Science. 282, 1318 (1998).

18. Chipuk, J. E. *et al.* Direct activation of Bax by p53 mediates mitochondrial membrane permeabilization and apoptosis. Science. 303, 1010 (2004).

19. Chu, A. & Stefani, E. Phosphatidylinositol 4,5-bisphosphate-induced Ca2+ release from skeletal muscle sarcoplasmic reticulum terminal cisternal membranes. Ca2+ flux and single channel studies. J. Biol. Chem. 266, 7699 (1991).

20. Conn, P. J. & Sanders-Bush, E. Selective 5HT-2 antagonists inhibit serotonin stimulated phosphatidylinositol metabolism in cerebral cortex. Neuropharmacology. 23, 993 (1984).

21. Constantinescu, A. *et al.* cAMP-dependent protein kinase type I regulates ethanol-induced cAMP response element-mediated gene expression via activation of CREB-binding protein and inhibition of MAPK. J. Biol. Chem. 279, 43321 (2004).

22. Cooper, D. M. *et al.* Adenosine receptor-mediated inhibition of rat cerebral cortical adenylate cyclase by a GTP-dependent process. Mol. Pharmacol. 18, 598 (1981).

23. Crespo, P. *et al.* Phosphotyrosine-dependent activation of Rac-1 GDP/GTP exchange by the vav proto-oncogene product. Nature. 385, 169 (1997).

24. Crespo, P. *et al.* Ras-dependent activation of MAP kinase pathway mediated by G-protein beta gamma subunits. Nature. 369, 418 (1994).

25. Cross, D. A. *et al.* Inhibition of glycogen synthase kinase-3 by insulin mediated by protein kinase B. Nature. 378, 785 (1996).

26. Cully, M. *et al.* Beyond PTEN mutations: The PI3K pathway as an integrator of multiple inputs during tumorigenesis. Nature Rev. Cancer. 6, 184 (2006).

27. D'Ambrosio, C. *et al.* Hyperphosphorylation of JNK-interacting protein 1, a protein associated with Alzheimer disease. Mol. Cell. Proteomics. 5, 97 (2006).

28. De Vivo, M. & Maayani, S. Characterization of the 5-hydroxytryptamine1a receptor-mediated inhibition of forskolin-stimulated adenylate cyclase activity in guinea pig and rat hippocampal membranes. J. Pharmacol. Exp. Ther. 238, 248 (1986).

29. De Waard, M. *et al.* Direct binding of G-protein betagamma complex to voltage-dependent calcium channels. Nature. 385, 446 (1997).

30. Delcommenne, M. *et al.* Phosphoinositide-3-OH kinase-dependent regulation of glycogen synthase kinase 3 and protein kinase B/AKT by the integrin-linked kinase. Proc. Natl. Acad. Sci. U. S. A. 95, 11211 (1998).

31. Deng, Y. *et al.* Growth factor receptor-binding protein 10 (Grb10) as a partner of phosphatidylinositol 3-kinase in metabolic insulin action. J. Biol. Chem. 278, 39311 (2003).

32. DeRemer, M. F. *et al.* $Ca(^{2+})$-calmodulin-dependent protein kinases Ia and Ib from rat brain. II. Enzymatic characteristics and regulation of activities by phosphorylation and dephosphorylation. J. Biol. Chem. 267, 13466 (1992).

33. Dessauer, C. W. *et al.* Identification of a Gialpha binding site on type V adenylyl cyclase. J. Biol. Chem. 273, 25831 (1998).

34. Dickens, M. *et al.* A cytoplasmic inhibitor of the JNK signal transduction pathway. Science. 277, 693 (1997).

35. Dutil, E. M. *et al.* Regulation of conventional protein kinase C isozymes by phosphoinositide-dependent kinase 1 (PDK-1). Curr. Biol. 8, 1366 (1999).

36. Edelman, A. M. *et al.* Multiple $Ca(^{2+})$-calmodulin-dependent protein kinase kinases from rat brain. Purification, regulation by $Ca(^{2+})$-calmodulin, and partial amino acid sequence. J. Biol. Chem. 271, 10806 (1996).

37. Enslen, H. *et al.* Characterization of Ca^{2+}/calmodulin-dependent protein kinase IV. Role in transcriptional regulation. J. Biol. Chem. 269, 15520 (1994).

38. Evan, G. I. & Vousden, K. H. Proliferation, cell cycle and apoptosis in cancer. Nature. 411, 342 (2001).

39. Feinstein, P. G. *et al.* Molecular cloning and characterization of a Ca2+/calmodulin-insensitive adenylyl cyclase from rat brain. Proc. Natl. Acad. Sci. U. S. A. 88, 10173 (1991).

40. Fiol, C. J. *et al.* A secondary phosphorylation of CREB341 at Ser129 is required for the cAMP-mediated control of gene expression. A role for glycogen synthase kinase-3 in the control of gene expression. J. Biol. Chem. 269, 32187 (1995).

41. Foulkes, N. S. *et al.* CREM gene: use of alternative DNA-binding domains generates multiple antagonists of cAMP-induced transcription. Cell. 64, 739 (1991).

42. Fukunaga, K. *et al.* Decreased protein phosphatase 2A activity in hippocampal long-term potentiation. J. Neurochem. 74, 807 (2000).

43. Giancotti, F. G. & Ruoslahti, E. Integrin signaling. Science. 285, 1028 (1999).

44. Goode, N. *et al.* Differential regulation of glycogen synthase kinase-3 beta by protein kinase C isotypes. J. Biol. Chem. 267, 16878 (1992).

45. Grilli, M. *et al.* Pharmacological characterization of D1 and D2 dopamine receptors in rat limbocortical areas. II. Dorsal hippocampus. Neurosci. Lett. 87, 253 (1988).

46. Gurd, J. W. & Bissoon, N. The N-methyl-D-aspartate receptor subunits NR2A and NR2B bind to the SH2 domains of phospholipase C-gamma. J. Neurochem. 69, 623 (1997).

47. Hadari, Y. R. *et al.* Insulin and insulinomimetic agents induce activation of phosphatidylinositol 3'-kinase upon its association with pp185 (IRS-1) in intact rat livers. J. Biol. Chem. 267, 17483 (1992).

48. Hai, T. & Curran, T. Cross-family dimerization of transcription factors Fos/Jun and ATF/CREB alters DNA binding specificity. Proc. Natl. Acad. Sci. U. S. A. 88, 3720 (1991).

49. Han, J. *et al.* Role of substrates and products of PI 3-kinase in regulating activation of Rac-related guanosine triphosphatases by Vav. Science. 279, 558 (1998).

50. Harris, S. L. & Levine, A. J. The p53 pathway: Positive and negative feedback loops. Oncogene. 24, 2899 (2005).

51. Hess, S. D. *et al.* Cloning and functional characterization of human heteromeric N-methyl-D-aspartate receptors. J. Pharmacol. Exp. Ther. 278, 808 (1996).

52. Hilgemann, D. W. *et al.* The complex and intriguing lives of PIP2 with ion channels and transporters. Sci. STKE. 2001, RE19, (2001).

53. Hillman, D. *et al.* Localization of P-type calcium channels in the central nervous system. Proc. Natl. Acad. Sci. U. S. A. 88, 7076 (1991).

54. Holgado-Madruga, M. *et al.* A Grb2-associated docking protein in EGF- and insulin-receptor signalling. Nature. 379, 560 (1996).

55. Holland, S. J. *et al.* Juxtamembrane tyrosine residues couple the Eph family receptor EphB2/Nuk to specific SH2 domain proteins in neuronal cells. EMBO. J. 16, 3877 (1997).

56. Hong, W. *et al.* Physical and functional interaction between the transcriptional cofactor CBP and the KH domain protein Sam68. Mol. Cancer. Res. 1, 48 (2002).

57. Hongpaisan, J. *et al.* Calcium-dependent mitochondrial superoxide modulates nuclear CREB phosphorylation in hippocampal neurons. Mol. Cell. Neurosci. 24, 1103 (2003).

58. Hu, B. *et al.* A critical interplay between Ca2+ inhibition and activation by Mg2+ of AC5 revealed by mutants and chimeric constructs. J. Biol. Chem. 277, 33139 (2002).

59. Imagawa, T. *et al.* Purified ryanodine receptor from skeletal muscle sarcoplasmic reticulum is the Ca2+-permeable pore of the calcium release channel. J. Biol. Chem. 262, 16636 (1988).

60. Ishikawa, Y. *et al.* Isolation and characterization of a novel cardiac adenylylcyclase cDNA. J. Biol. Chem. 267, 13553 (1992).

61. Jensen, C. J. *et al.* 90-kDa ribosomal S6 kinase is phosphorylated and activated by 3-phosphoinositide-dependent protein kinase-1. J. Biol. Chem. 274, 27168 (1999).

62. Kajikawa, Y. *et al.* GTP-binding protein beta gamma subunits mediate presynaptic calcium current inhibition by GABA(B) receptor. Proc. Natl. Acad. Sci. U. S. A. 98, 8054 (2001).

63. Kameshita, I. & Fujisawa, H. Autophosphorylation of calmodulin-dependent protein kinase IV from rat cerebral cortex. J. Biochem. (Tokyo). 113, 583 (1993).

64. Kapoor, G. S. *et al.* Distinct domains in the SHP-2 phosphatase differentially regulate epidermal growth factor receptor/NF-kappaB activation through Gab1 in glioblastoma cells. Mol. Cell. Biol. 24, 823 (2003).

65. Kasahara, J. *et al.* Differential effects of a calcineurin inhibitor on glutamate-induced phosphorylation of Ca^{2+}/calmodulin-dependent protein kinases in cultured rat hippocampal neurons. J. Biol. Chem. 274, 9061 (1999).

66. Kaupmann, K. *et al.* Expression cloning of GABA(B) receptors uncovers similarity to metabotropic glutamate receptors. Nature. 386, 239 (1997).

67. Kawabe, J. *et al.* Differential activation of adenylyl cyclase by protein kinase C isoenzymes. J. Biol. Chem. 269, 16554 (1994).

68. Kazlauskas, A. & Cooper, J. A. Autophosphorylation of the PDGF receptor in the kinase insert region regulates interactions with cell proteins. Cell. 58, 1121 (1989).

69. Kim, U. H. *et al.* Phosphorylation of phospholipase C-gamma by cAMP-dependent protein kinase. J. Biol. Chem. 264, 20167 (1990).

70. Klee, C. B. *et al.* Calcineurin: a calcium- and calmodulin-binding protein of the nervous system. Proc. Natl. Acad. Sci. U. S. A. 76, 6270 (1980).

71. Kobilka, B. K. *et al.* An intronless gene encoding a potential member of the family of receptors coupled to guanine nucleotide regulatory proteins. Nature. 329, 75 (1987).

72. Kong, M. *et al.* The PP2A-associated protein alpha4 is an essential inhibitor of apoptosis. Science. 306, 695 (2004).

73. Kozasa, T. & Gilman, A. G. Purification of recombinant G proteins from Sf9 cells by hexahistidine tagging of associated subunits. Characterization of alpha 12 and inhibition of adenylyl cyclase by alpha z. J. Biol. Chem. 270, 1734 (1995).

74. Lee, C. H. *et al.* Nck associates with the SH2 domain-docking protein IRS-1 in insulin-stimulated cells. Proc. Natl. Acad. Sci. U. S. A. 90, 11713 (1994).

75. Leonard, A. S. & Hell, J. W. Cyclic AMP-dependent protein kinase and protein kinase C phosphorylate N-methyl-D-aspartate receptors at different sites. J. Biol. Chem. 272, 12107 (1997).

76. Leonard, A. S. *et al.* Regulation of calcium/calmodulin-dependent protein kinase II docking to N-methyl-D-aspartate receptors by calcium/calmodulin and alpha-actinin. J. Biol. Chem. 277, 48441 (2002).

77. Li, A. G. *et al.* Mechanistic insights into maintenance of high p53 acetylation by PTEN. Mol Cell. 23, 575 (2006).

78. Li, P. *et al.* Cytochrome c and dATP-dependent formation of Apaf-1/caspase-9 complex initiates an apoptotic protease cascade. Cell. 91, 479 (1997).

79. Libert, F. *et al.* Selective amplification and cloning of four new members of the G protein-coupled receptor family. Science. 244, 569 (1989).

80. Lieberman, D. N. & Mody, I. Regulation of NMDA channel function by endogenous Ca($^{2+}$)-dependent phosphatase. Nature. 369, 235 (1994).

81. Litosch, I. Protein kinase C inhibits the Ca(2+)-dependent stimulation of phospholipase C-beta 1 in vitro. Recept. Signal. Transduct. 6, 87 (1997).

82. Liu, M. & Simon, M. I. Regulation by cAMP-dependent protein kinase of a G-protein-mediated phospholipase C. Nature. 382, 83 (1996).

83. Look, T. Oncogenic transcription factors in the human acute leukemias. Science. 278, 1059 (1997).

84. Lowe, S. W. *et al.* Intrinsic tumour suppression. Nature. 432, 307 (2004).

85. Lu, W. *et al.* Activation of Pak by membrane localization mediated by an SH3 domain from the adaptor protein Nck. Curr. Biol. 7, 85 (1997).

86. MacDermott, A. B. *et al.* NMDA-receptor activation increases cytoplasmic calcium concentration in cultured spinal cord neurones. Nature. 321, 519 (1986).

87. Madison, D. V. *et al.* Phorbol esters block a voltage-sensitive chloride current in hippocampal pyramidal cells. Nature. 321, 695 (1986).

88. Manser, E. *et al.* A brain serine/threonine protein kinase activated by Cdc42 and Rac1. Nature. 367, 40 (1994).

89. Masu, M. *et al.* Sequence and expression of a metabotropic glutamate receptor. Nature. 349, 760 (1991).

90. Matoba, S. *et al.* p53 regulates mitochondrial respiration. Science. 312, 1650 (2006).

91. Matsushita, M. & Nairn, A. C. Inhibition of the Ca^{2+}/calmodulin-dependent protein kinase I cascade by cAMP-dependent protein kinase. J. Biol. Chem. 274, 10086 (1999).

92. McCullar, J. S. *et al.* Calmodulin is a phospholipase C-beta interacting protein. J. Biol. Chem. 278, 33708 (2003).

93. Meisenhelder, J. *et al.* Phospholipase C-gamma is a substrate for the PDGF and EGF receptor protein-tyrosine kinases in vivo and in vitro. Cell. 57, 1109 (1989).

94. Mejillano, M. *et al.* Regulation of apoptosis by phosphatidylinositol 4,5-bisphosphate inhibition of caspases, and caspase inactivation of phosphatidylinositol phosphate 5-kinases. J. Biol. Chem. 276, 1865 (2001).

95. Miller, S. G. & Kennedy, M. B. Regulation of brain type II Ca^{2+}/calmodulin-dependent protein kinase by autophosphorylation: a Ca^{2+}-triggered molecular switch. Cell. 44, 861 (1986).

96. Moeschel, K. *et al.* Protein kinase C-zeta-induced phosphorylation of Ser318 in insulin receptor substrate-1 (IRS-1) attenuates the interaction with the insulin receptor and the tyrosine phosphorylation of IRS-1. J. Biol. Chem. 279, 25157 (2004).

97. Montminy, M. R. *et al.* Identification of a cyclic-AMP-responsive element within the rat somatostatin gene. Proc. Natl. Acad. Sci. U. S. A. 83, 6682 (1986).

98. Mora, A. *et al.* Lithium blocks the PKB and GSK3 dephosphorylation induced by ceramide through protein phosphatase-2A. Cell. Signal. 14, 557 (2002).

99. Mussig, K. *et al.* Shp2 is required for protein kinase C-dependent phosphorylation of serine 307 in insulin receptor substrate-1. J. Biol. Chem. 280, 32693 (2005).

100. Najib, S. & Sanchez-Margalet, V. Sam68 associates with the SH3 domains of Grb2 recruiting GAP to the Grb2-SOS complex in insulin receptor signaling. J. Cell. Biochem. 86, 99 (2002).

101. Nakagawa, O. *et al.* ROCK-I and ROCK-II, two isoforms of Rho-associated coiled-coil forming protein serine/threonine kinase in mice. FEBS. Lett. 392, 189 (1996).

102. Nakajima, Y. *et al.* A relationship between protein kinase C phosphorylation and calmodulin binding to the metabotropic glutamate receptor subtype 7. J. Biol. Chem. 274, 27573 (1999).

103. Nicholson, D. W. From bench to clinic with apoptosis-based therapeutic agents. Nature. 407, 810 (2000).

104. Nie, Y. *et al.* Stimulation of p53 DNA binding by c-Abl requires the p53 C terminus and tetramerization. Mol. Cell. Biol. 20, 741 (2000).

105. Niggli, V. *et al.* Acidic phospholipids, unsaturated fatty acids, and limited proteolysis mimic the effect of calmodulin on the purified erythrocyte Ca2+ -ATPase. J. Biol. Chem. 256, 8588 (1981).

106. Obadiah, J. *et al.* Adenylyl cyclase interaction with the D2 dopamine receptor family; differential coupling to Gi, Gz, and Gs. Cell. Mol. Neurobiol. 19, 653 (1999).

107. Olah, M. E. Identification of A2a adenosine receptor domains involved in selective coupling to Gs. Analysis of chimeric A1/A2a adenosine receptors. J. Biol. Chem. 272, 337 (1997).

108. Oldenhof, J. *et al.* SH3 ligands in the dopamine D3 receptor. Cell. Signal. 13, 411 (2001).

109. Olson, M. F. *et al.* Faciogenital dysplasia protein (FGD1) and Vav, two related proteins required for normal embryonic development, are upstream regulators of Rho GTPases. Curr. Biol. 6, 1628 (1997).

110. Persad, S. *et al.* Inhibition of integrin-linked kinase (ILK) suppresses activation of protein kinase B/Akt and induces cell cycle arrest and apoptosis of PTEN-mutant prostate cancer cells. Proc. Natl. Acad. Sci. U. S. A. 97, 3207 (2000).

111. Ren, X. D. *et al.* Physical association of the small GTPase Rho with a 68-kDa phosphatidylinositol 4-phosphate 5-kinase in Swiss 3T3 cells. Mol. Biol. Cell. 7, 435 (1996).

112. Rich, T. *et al.* Defying death after DNA damage. Nature. 407, 777 (2000).

113. Roig, J. *et al.* Functional interaction between c-Abl and the p21-activated protein kinase gamma-PAK. Proc. Natl. Acad. Sci. U. S. A. 97, 14346 (2001).

114. Ross, C. A. *et al.* Three additional inositol 1,4,5-trisphosphate receptors: molecular cloning and differential localization in brain and peripheral tissues. Proc. Natl. Acad. Sci. U. S. A. 89, 4265 (1992).

115. Ross, E. M. *et al.* Reconstitution of hormone-sensitive adenylate cyclase activity with resolved components of the enzyme. J. Biol. Chem. 253, 6401 (1978).

116. Runnels, L. W. *et al.* The TRPM7 channel is inactivated by PIP(2) hydrolysis. Nat. Cell. Biol. 4, 329 (2002).

117. Santoro, M. F. *et al.* Regulation of protein phosphatase 2A activity by caspase-3 during apoptosis. J. Biol. Chem. 273, 13119 (1998).

118. Sato, M. *et al.* Altered agonist sensitivity and desensitization of neuronal mGluR1 responses in knock-in mice by a single amino acid substitution at the PKC phosphorylation site. Eur. J. Neurosci. 20, 947 (2004).

119. Sawyers, C. Targeted cancer therapy. Nature. 432, 294 (2004).

120. Schuebel, K. E. *et al.* Phosphorylation-dependent and constitutive activation of Rho proteins by wild-type and oncogenic Vav-2. EMBO. J. 17, 6608 (1999).

121. Shaw, R. J. & Cantley, L. C. Ras, PI(3)K and mTOR signalling controls tumour cell growth. Nature. 441, 424 (2006).

122. Sheng, M. *et al.* CREB: a Ca($^{2+}$)-regulated transcription factor phosphorylated by calmodulin-dependent kinases. Science. 252, 1427 (1991).

123. Sidhu, A. *et al.* D1 dopamine receptors can interact with both stimulatory and inhibitory guanine nucleotide binding proteins. J. Neurochem. 57, 1445 (1991).

124. Singh, S. S. *et al.* Activation of protein kinase C by phosphatidylinositol 3,4,5-trisphosphate. Biochem. Biophys. Res. Commun. 195, 104 (1993).

125. Skeen, J. E. *et al.* Akt deficiency impairs normal cell proliferation and suppresses oncogenesis in a p53-independent and mTORC1-dependent manner. Cancer Cell. 10, 269 (2006).

126. Skolnik, E. Y. *et al.* The SH2/SH3 domain-containing protein GRB2 interacts with tyrosine-phosphorylated IRS1 and Shc: implications for insulin control of ras signalling. EMBO. J. 12, 1929 (1993).

127. Smith, J. M. *et al.* Activation of the Abl tyrosine kinase in vivo by Src homology 3 domains from the Src homology 2/Src homology 3 adaptor Nck. J. Biol. Chem. 274, 27956 (1999).

128. Soengas, M. S. *et al.* Apaf-1 and Caspase-9 in p53-dependent apoptosis and tumor inhibition. Science. 284, 156 (1999).

129. Sorensen, S. D. *et al.* Dissociation of protein kinase-mediated regulation of metabotropic glutamate receptor 7 (mGluR7) interactions with calmodulin and regulation of mGluR7 function. Mol. Pharmacol. 61, 1303 (2002).

130. Srinivasula, S. M. *et al.* Molecular ordering of the Fas-apoptotic pathway: the Fas/APO-1 protease Mch5 is a CrmA-inhibitable protease that activates multiple Ced-3/ICE-like cysteine proteases. Proc. Natl. Acad. Sci. U. S. A. 93, 14486 (1997).

131. Stahl, M. L. *et al.* Sequence similarity of phospholipase C with the non-catalytic region of src. Nature. 332, 269 (1988).

132. Stephens, L. *et al.* A novel phosphoinositide 3 kinase activity in myeloid-derived cells is activated by G protein beta gamma subunits. Cell. 77, 83 (1994).

133. Stephens, L. *et al.* Protein kinase B kinases that mediate phosphatidylinositol 3,4,5-trisphosphate-dependent activation of protein kinase B. Science. 279, 710 (1998).

134. Sugimoto, S. *et al.* Expression, purification, and characterization of SH2-containing protein tyrosine phosphatase, SH-PTP2. J. Biol. Chem. 268, 22771 (1993).

135. Sugiyama, H. *et al.* Glutamate receptor subtypes may be classified into two major categories: a study on Xenopus oocytes injected with rat brain mRNA. Neuron. 3, 129 (1990).

136. Sun, X. *et al.* Interaction between protein kinase C delta and the c-Abl tyrosine kinase in the cellular response to oxidative stress. J. Biol. Chem. 275, 7470 (2000).

137. Sun, X. J. *et al.* Expression and function of IRS-1 in insulin signal transmission. J. Biol. Chem. 267, 22662 (1992).

138. Sun, Z. *et al.* Calspermin gene transcription is regulated by two cyclic AMP response elements contained in an alternative promoter in the calmodulin kinase IV gene. Mol. Cell. Biol. 15, 561 (1995).

139. Supattapone, S. *et al.* Cyclic AMP-dependent phosphorylation of a brain inositol trisphosphate receptor decreases its release of calcium. Proc. Natl. Acad. Sci. U. S. A. 85, 8747 (1988).

140. Swartz, K. J. *et al.* Protein kinase C modulates glutamate receptor inhibition of Ca^{2+} channels and synaptic transmission. Nature. 361, 165 (1993).

141. Takai, Y. *et al.* Calcium-dependent activation of a multifunctional protein kinase by membrane phospholipids. J. Biol. Chem. 254, 3692 (1979).

142. Tang, W. J. & Gilman, A. G. Type-specific regulation of adenylyl cyclase by G protein beta gamma subunits. Science. 254, 1500 (1992).

143. Tang, W. J. *et al.* Expression and characterization of calmodulin-activated (type I) adenylylcyclase. J. Biol. Chem. 266, 8595 (1991).

144. Tauchi, T. *et al.* The ubiquitously expressed Syp phosphatase interacts with c-kit and Grb2 in hematopoietic cells. J. Biol. Chem. 269, 25206 (1994).

145. Taussig, R. *et al.* Inhibition of adenylyl cyclase by Gi alpha. Science. 261, 218 (1993).

146. Tingley, W. G. *et al.* Regulation of NMDA receptor phosphorylation by alternative splicing of the C-terminal domain. Nature. 364, 70 (1993).

147. Torres, J. *et al.* Phosphorylation-regulated cleavage of the tumor suppressor PTEN by caspase-3: implications for the control of protein stability and PTEN-protein interactions. J. Biol. Chem. 278, 30652 (2003).

148. Usachev, Y. M. *et al.* Bradykinin and ATP accelerate Ca(2+) efflux from rat sensory neurons via protein kinase C and the plasma membrane Ca(2+) pump isoform 4. Neuron. 33, 113 (2002).

149. van Houten, M. *et al.* Insulin binding sites localized to nerve terminals in rat median eminence and arcuate nucleus. Science. 207, 1081 (1980).

150. van Koppen, C. J. *et al.* Isolation, sequence and functional expression of the mouse m4 muscarinic acetylcholine receptor gene. Biochim. Biophys. Acta. 1173, 342 (1993).

151. Vivanco, I. & Sawyers, C. L. The phosphatidylinositol 3-Kinase AKT pathway in human cancer. Nature Rev. Cancer. 2, 489 (2002).

152. Wadzinski, B. E. *et al.* Nuclear protein phosphatase 2A dephosphorylates protein kinase A-phosphorylated CREB and regulates CREB transcriptional stimulation. Mol. Cell. Biol. 13, 2822 (1993).

153. Wang, L. Y. *et al.* Regulation of NMDA receptors in cultured hippocampal neurons by protein phosphatases 1 and 2A. Nature. 369, 230 (1994).

154. Watterson, D. M. *et al.* The complete amino acid sequence of the Ca^{2+}-dependent modulator protein (calmodulin) of bovine brain. J. Biol. Chem. 255, 962 (1980).

155. Wei, W. *et al.* The v-Jun point mutation allows c-Jun to escape GSK3-dependent recognition and destruction by the Fbw7 ubiquitin ligase. Cancer. Cell. 8, 25 (2005).

156. Welham, M. J. *et al.* Interleukin (IL)-3 and granulocyte/macrophage colony-stimulating factor, but not IL-4, induce tyrosine phosphorylation, activation, and association of SHPTP2 with Grb2 and phosphatidylinositol 3'-kinase. J. Biol. Chem. 269, 23764 (1994).

157. Westenbroek, R. E. *et al.* Biochemical properties and subcellular distribution of an N-type calcium channel alpha 1 subunit. Neuron. 9, 1099 (1993).

158. Westphal, R. S. *et al.* A signaling complex of Ca^{2+}-calmodulin-dependent protein kinase IV and protein phosphatase 2A. Science. 280, 1258 (1998).

159. Whitman, M. *et al.* Type I phosphatidylinositol kinase makes a novel inositol phospholipid, phosphatidylinositol-3-phosphate. Nature. 332, 644 (1988).

160. Wu, L. *et al.* Dual regulation of voltage-gated calcium channels by PtdIns(4,5)P2. Nature. 419, 947 (2002).

161. Xia, Z. *et al.* Type I calmodulin-sensitive adenylyl cyclase is neural specific. J. Neurochem. 60, 305 (1993).

162. Xing, J. *et al.* Coupling of the RAS-MAPK pathway to gene activation by RSK2, a growth factor-regulated CREB kinase. Science. 273, 959 (1996).

163. Xu, N. *et al.* The PH domain of Ras-GAP is sufficient for in vitro binding to beta gamma subunits of heterotrimeric G proteins. Cell. Mol. Neurobiol. 16, 51 (1996).

164. Yabana, N. & Shibuya, M. Adaptor protein APS binds the NH2-terminal autoinhibitory domain of guanine nucleotide exchange factor Vav3 and augments its activity. Oncogene. 21, 7720 (2002).

165. Yamada, M. *et al.* Insulin receptor substrate (IRS)-1 and IRS-2 are tyrosine-phosphorylated and associated with phosphatidylinositol 3-kinase in response to brain-derived neurotrophic factor in cultured cerebral cortical neurons. J. Biol. Chem. 272, 30334 (1997).

166. Yamaguchi, A. *et al.* Akt activation protects hippocampal neurons from apoptosis by inhibiting transcriptional activity of p53. J. Biol. Chem. 276, 5256 (2001).

167. Yamanashi, Y. & Baltimore, D. Identification of the Abl- and rasGAP-associated 62 kDa protein as a docking protein, Dok. Cell. 88, 205 (1997).

168. Yan, Z. & Surmeier, D. J. Muscarinic (m2/m4) receptors reduce N- and P-type Ca^{2+} currents in rat neostriatal cholinergic interneurons through a fast, membrane-delimited, G-protein pathway. J. Neurosci. 16, 2592 (1996).

169. Yang, M. *et al.* Requirement of Gbetagamma and c-Src in D2 dopamine receptor-mediated nuclear factor-kappaB activation. Mol. Pharmacol. 64, 447 (2003).

170. Yano, S. *et al.* Calcium promotes cell survival through CaM-K kinase activation of the protein-kinase-B pathway. Nature. 396, 584 (1999).

171. Ye, Z. S. & Baltimore, D. Binding of Vav to Grb2 through dimerization of Src homology 3 domains. Proc. Natl. Acad. Sci. U. S. A. 91, 12629 (1995).

172. Yokouchi, M. *et al.* APS, an adaptor protein containing PH and SH2 domains, is associated with the PDGF receptor and c-Cbl and inhibits PDGF-induced mitogenesis. Oncogene. 18, 759 (1999).

173. Yokoyama, C. T. *et al.* Phosphorylation of the synaptic protein interaction site on N-type calcium channels inhibits interactions with SNARE proteins. J. Neurosci. 17, 6929 (1997).

174. Yoshimura, M. & Cooper, D. M. Type-specific stimulation of adenylylcyclase by protein kinase C. J. Biol. Chem. 268, 4604 (1993).

175. Yue, Y. *et al.* Ras GTPase-activating protein binds to Akt and is required for its activation. J. Biol. Chem. 279, 12883 (2004).

176. Zamanillo, D. *et al.* Identification of a cyclic adenosine 3',5'-monophosphate-dependent protein kinase phosphorylation site in the carboxy terminal tail of human D1 dopamine receptor. Neurosci. Lett. 188, 183 (1995).

177. Zylinska, L. *et al.* Protein kinases A and C phosphorylate purified Ca2+-ATPase from rat cortex, cerebellum and hippocampus. Biochim. Biophys. Acta. 1448, 99 (1999).